# GAS PRESSURE MEASUREMENTS ON SPACE SHUTTLE MISSION-39

William F. Denig
Rodney Viereck

9 April 1996

19970602 050

**PHILLIPS LABORATORY**
Directorate of Geophysics
**AIR FORCE MATERIEL COMMAND**
**HANSCOM AIR FORCE BASE, MA 01731-3010**

DTIC QUALITY INSPECTED 1

# GAS PRESSURE MEASUREMENTS ON SPACE SHUTTLE MISSION-39

William F. Denig
Rodney A. Viereck

9 April 1996

# ERRATA

The printed copies of subject report show an incorrect TR number on the cover and documentation page as PL-TR-96-2101. <u>The correct number for this report should read PL-TR-96-2102</u>
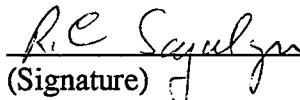
"This technical report has been reviewed and is approved for publication"


_EG Mullen_ (signature)

(Signature)
E.G. MULLEN
Branch Chief

_RC Sagalyn_ (signature)

(Signature)
R.C. SAGALYN
Division Director


This report has been reviewed by the ESC Public Affairs Office (PA) and is releasable to the National Technical Information Service (NTIS).

Qualified requestors may obtain additional copies from the Defense Technical Information Center (DTIC). All others should apply to the National Technical Information Service (NTIS).

If your mailing address has changed, if you wish to be removed from the mailing list, or if thge addressee is no longer employed by your organization, please notify PL/IM, 29 Randolph Road, Hanscom AFB, MA 01731-3010. This will assist us in maintaining a current mailing list.

Do not return copies of this report unless contractual obligations or notices on a specific document require that it be returned.

# REPORT DOCUMENTATION PAGE

Public reporting burden for this collection of information is estimated to average 1 hour per response, including the time for reviewing instructions, searching existing data sources, gathering and maintaining the data needed, and completing and reviewing the collection of information. Send comments regarding this burden estimate or any other aspect of this collection of information, including suggestions for reducing this burden, to Washington Headquarters Services, Directorate for Information Operations and Reports, 1215 Jefferson Davis Highway, Suite 1204, Arlington, VA 22202-4302, and to the Office of Management and Budget, Paperwork Reduction Project (0704-0188), Washington, DC 20503.

| 1. AGENCY USE ONLY (Leave blank) | 2. REPORT DATE 9 April 1996 | 3. REPORT TYPE AND DATES COVERED Scientific, Interim |
|---|---|---|

**4. TITLE AND SUBTITLE**

Gas Pressure Measurements on Space Shuttle Mission-39

**6. AUTHOR(S)**

William F. Denig, Rodney A. Viereck

**5. FUNDING NUMBERS**

PE 63410F
Proj: 2822
Task: 282201
Work Unit: 28220101

**7. PERFORMING ORGANIZATION NAME(S) AND ADDRESS(ES)**

Phillips Laboratory/GPSP
29 Randolph Road
Hanscom AFB, MA 01731-3010

**8. PERFORMING ORGANIZATION REPORT NUMBER**

PL-TR-96-2101
IP, No. 348

**9. SPONSORING / MONITORING AGENCY NAME(S) AND ADDRESS(ES)**

**10. SPONSORING / MONITORING AGENCY REPORT NUMBER**

**11. SUPPLEMENTARY NOTES**

**12a. DISTRIBUTION / AVAILABILITY STATEMENT**

Approved for public release;
Distribution unlimited

**12b. DISTRIBUTION CODE**

**13. ABSTRACT** (Maximum 200 words)

During the STS-39 Space Shuttle Mission in April 1991 a Neutral gas pressure gauge was flown as part of the Infrared Background Signature Survey (IBSS) mission. This instrument provided gas pressure measurements within the Shuttle payload bay, on the Remote Manipulator System (RMS) arm, and as part of a deployed Shuttle PAllet Satellite (SPAS). The Presure Gauge (PG) was found to be sensitive to payload bay outgassing, controlled gas releases, and geometry. During the 7-day mission the in-bay pressures decreased about an order of magnitude from $2 \times 10^{-6}$ to $3 \times 10^{-7}$ Torr. Local gas pressures were found to be dependent upon the availability of scattering surfaces within the field-of-view and the orientation of the Shuttle ram angle. On the other hand, SPAS pressures were consistent with background atmospheric levels near $10^{-8}$ Torr. At all time the local pressures were found to be sensitive to attitude control thruster operations and other controlled gas releases. The STS-39 pressure measurements indicate that the persistently high levels of contaminant gases within the cargo bay were larger than those measured on most earlier Shuttle missions and greater than NASA contaminant gas specifications.

**14. SUBJECT TERMS**

Spacecraft environment, Pressure Gauge, Spacecraft contamination

**15. NUMBER OF PAGES** 56

**16. PRICE CODE**

| 17. SECURITY CLASSIFICATION OF REPORT Unclassified | 18. SECURITY CLASSIFICATION OF THIS PAGE Unclassified | 19. SECURITY CLASSIFICATION OF ABSTRACT Unclassified | 20. LIMITATION OF ABSTRACT SAR |
|---|---|---|---|

# Contents

# Illustrations

# Tables

# Acknowledgements

# Gas Pressure Measurements on Space Shuttle Mission-39

## 1. INTRODUCTION

The primary purposes of the Infrared Background Signature Survey (IBSS) experiments on Space Shuttle mission STS-29 were; 1) to measure the optical radiative signatures from controlled gas releases and from naturally-occurring atmosphere emissions and 2) to determine the deleterious effects of the orbiter environment on these signatures. The IBSS hardware for making these measurements consisted of a complement of optical instrumentation covering the light spectrum from the near ultraviolet to the infrared. Background measurements were made of the airglow and the aurora while active experiments involved operations of the Shuttle's attitude and orbital control jet engines and orchestrated chemical releases from on-board and deployed gas canisters. The principal instruments making up the IBSS were a pair of Low-Light-Level Television ($L^3TV$) cameras, a visible and near-ultraviolet imager/spectrograph, and a cryogenically-cooled infrared radiometer/spectrometer. Also included as part of the IBSS payload was a neutral gas Pressure Gauge (PG) sensitive within the range $10^{-3}$-to-$10^{-8}$ Torr. The IBSS PG was designed to assist in the analysis of the optical data by measuring neutral gas contamination near the sensitive optical instrumentation. This contamination resulted from the controlled experiments and incidental conditions that affected the local neutral gas environment. This report is a comprehensive discussion of the IBSS PG for mission STS-39 covering the development, calibration, and flight data of the instrument.

The IBSS was launched on April 28, 1991 aboard the Space Shuttle Discovery, as one of three primary payloads. The accompanying payloads for STS-39 were the AFP-675 [*Ahmadjian et al.*, 1990] and STP-1 [*Ahmadjian et al.*, 1992] which included the Cryogenics

Infrared Radiance Instrumentation for Shuttle (CIRRIS) and the Spacecraft Kinetic InfraRed Test (SKIRT), respectively. The Shuttle was inserted into a 57° inclination orbit at an altitude of 260 km for a mission that lasted 8 days. The IBSS experiments were mounted on a Shuttle PAllet Satellite (SPAS) that was deployed from the cargo bay by the Remote Manipulator System (RMS) and released as a recoverable free flyer. During the Shuttle mission pressure data were obtained within the bay, while the SPAS was attached to the RMS, and on the released SPAS.

The neutral gas environment surrounding a spacecraft consists of gases of atmospheric origin and locally produced contamination. Local sources of contamination are vehicle and payload outgassing and gaseous releases from pressure vessel purging and rocket engine exhausts. The effects of these contaminant sources can often be minimized by paying careful attention to material selection, assembly procedures and spacecraft design. On satellites the deleterious effects of contamination can be further minimized by allowing ample time; that is, weeks to months, for material outgassing prior to operational use. Sounding rockets, on the other hand, often experience relatively high levels of outgassing because they must operate within a few minutes of launch [*Allred et al.*, 1988; *Goerke et al.*, 1992]. The Space Shuttle is a complex space system that is subject to gaseous contamination from numerous sources. The almost constant maneuvering of the Shuttle, coupled with the vast aggregate of potential outgassing sources makes a consideration of the Shuttle gaseous environment difficult [*Barengoltz*, 1985].

Over the years there have been numerous in-situ experiments designed to measure the gaseous contamination near the Shuttle [*Green et al.*, 1985; *Erlers et al.*, 1984; *Miller*, 1984; *Scialdone*, 1983; *von Zahn and Wulf*, 1985] An early assessment of the Shuttle neutral gas environment for mission STS-3 was reported by *Shawhan and Murphy* [1983]. These authors found that it took almost 24 hours for the background pressures, mostly from outgassing, to drop to near ambient levels. *Kawashima et al.* [1985], on the other hand, found that for the entire SpaceLab I mission the neutral density within the payload bay was at least a factor of 10 higher than the expected atmospheric levels of about $8 \times 10^{-8}$ Torr. Neutral pressures within the bay have been found to vary depending on vehicle attitude and on transient gas releases from Shuttle systems [ *Pickett et al.*, 1985; 1988]. *Shawhan et al.* [1984] suggested that their measurement of an attitude effect was caused by a surface chemical reaction resulting from the recombination of atmospheric atomic oxygen (*O*) near the gauge surface while *Kawashima et al.* [1985] maintain that the enhanced pressures were due to scattering of atmospheric gases within the cargo bay. There have also been numerous studies of the contamination

2

induced by the Shuttle's rocket engines used for attitude control and orbital maneuvering engines [*Erlers*, 1984; *Machuzak et al.*, 1993; *Hunton*, 1994]. Engine-related pressure spikes were investigated by *Narcisi et al.* [1983], *Wulf and von Zahn* [1986], and more recently, *Hunton* [1994] and *Hunton and Machuzak* [1994] who found that the observation and degree of these effects were, in general, related to an apparent scattering of the engine exhaust products from Shuttle surfaces. The purpose of this report is to contribute to this body of knowledge and to provide a record of the gaseous environment on the Space Shuttle for STS-39.

## 2. INSTRUMENT DESCRIPTION

The IBSS PG was developed as a spacecraft contamination sensor. The PG consisted of a cold-cathode ionization gauge and supporting electronics. Figure 1 is a schematic overview of the PG sensor unit, illustrating its overall configuration and internal structure. The PG sensor consisted of a commercially available Varian Model 524-2 Cold Cathode Vacuum Gauge that was modified for flight use. The cold cathode operated at 4.2 kVac within an effective magnetic field of 17.5 kGauss. All high voltages were contained within the sensor unit and the internal magnetic field was externally shielded by an arrangement of fixed compensation magnets. The telemetry output voltage for the gas sensor was logarithmically related to the pressure within an antechamber mounted forward of the Varian gauge aperture. The purpose of the antechamber was to provide a tractable geometry for which an analysis of aperture orientation relative to the ram-flowing gases could be achieved. The chamber also allowed the incoming atmospheric gases, primarily $O$, to be chemically accommodated prior to entering the cold cathode gauge and prevented spurious signals from charged particles entering the gauge. The IBSS PG was designed and fabricated at the SenTran Company of Santa Barbara by Mr. Peter Simeth under contract to the Johns Hopkins University Applied Physics Laboratory (JHU/APL).

### 2.1 Varian 524-2 Cold Cathode Vacuum Gauge

The Varian 524-2 cold cathode vacuum gauge is derived from the Redhead magnetron gauge which was developed as a laboratory instrument in the mid-to-late 50's [*Redhead*, 1959]. The magnetron gauge operates on the basic Penning discharge principle of crossed $\boldsymbol{E}$ and $\boldsymbol{B}$ fields whereby electrons created within the discharge region are trapped by their drift motion and the cylindrical geometry of the gauge. The helical trajectories of the electrons inhibit their radial flow
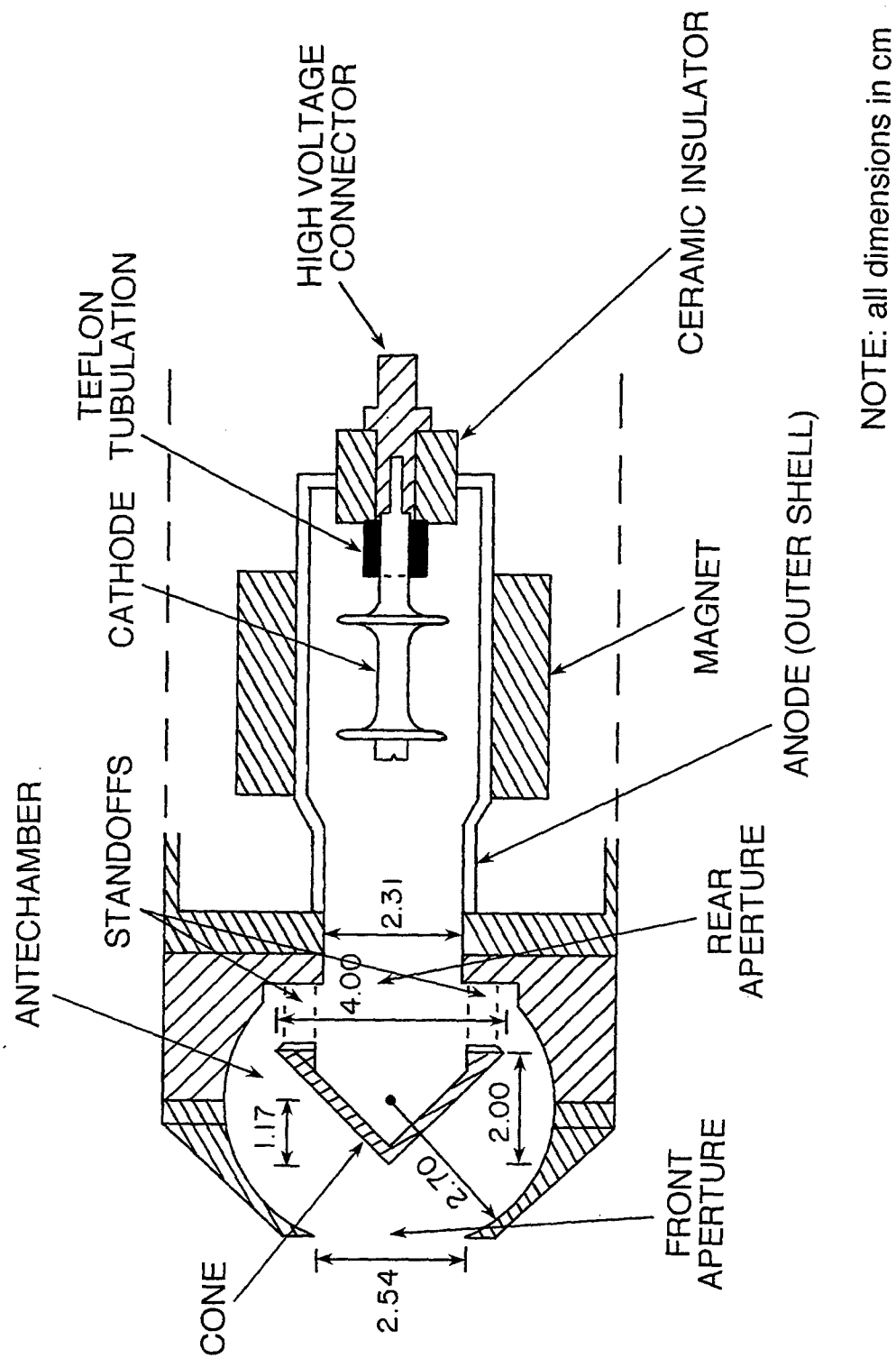
Figure 1. Schematic Drawing of the PG Antechamber and Cold-Cathode Gauge

HIGH VOLTAGE CONNECTOR

TEFLON TUBULATION

CATHODE

CERAMIC INSULATOR

MAGNET

ANODE (OUTER SHELL)

ANTECHAMBER

STANDOFFS

REAR APERTURE

FRONT APERTURE

CONE

2.31

4.00

2.00

1.17

2.70

2.54

NOTE: all dimensions in cm

4

within the gauge. The trapped electrons have a high probability of undergoing numerous ionizing collision with neutral gases within the gauge thereby sustaining the discharge. The more massive positive ions created within the gauge travel relatively unimpeded to the cathode and generate the sensor current. The cathode current is approximately linear over the range of $10^{-9}$-to-$10^{-3}$ Torr. A key advantage of the Redhead gauge over other cold-cathode configurations is its ability to ignite or "strike" at pressures as low as $10^{-8}$ Torr; that is, the internal electric fields are sufficient to create the seed ionization required to ignite the discharge.

Gauges similar in design to the IBSS PG have been flown on earlier Shuttle missions and sounding rocket flights. A 524-2 cold cathode gauge was included as part of the Plasma Diagnostic Package (PDP) on the OSS-1 (STS-3) and SpaceLab-2 (STS-51F) missions in 1982 and 1985, respectively [Pickett et al., 1985; 1988]. Cold-cathode gauges were also used to measure the contaminant background pressures on the SPEAR-2 and SCEX-3 rocket flights [Allred et al., 1988; Goerke et al., 1992] although there are indications that these rocket measurements may have been compromised by gauge outgassing [R. Erlandson, private communication, 1992]. However the IBSS PG was unique in that the instrument design included a spherical antechamber in place of a front baffle arrangement. For STS-39, pressure measurements were also made away from the main vehicle while the SPAS was deployed.

## 2.2 Antechamber Design

The IBSS PG was specifically configured to support Shuttle and SPAS measurements. To simplify measurements and calculations, the gauge was fitted with a forward-mounted antechamber designed to allow chemical accommodation of atmospheric $O$ and provide a simple internal geometry for modeling purposes. The antechamber also made the instrument less susceptible to incoming charged particles by limiting their direct access to the cathode. The PG antechamber was similar to an earlier design used for the ESRO 4 Gas Analyzer [Trinks and von Zahn, 1975].

The spherical antechamber, illustrated in detail in Figure 1, was 2.70 cm in radius and had a circular inlet aperture of 5.07 cm². A right circular cone [base=4.00 cm, height=2.00 cm] was mounted within the chamber above the outlet aperture to the Varian cold-cathode gauge on four supporting standoffs. This arrangement prevented direct access by the incoming particle fluxes to the cold cathode yet provided adequate "ventilation" to rapidly equalize the antechamber and gauge pressures. The cone standoffs were 0.99 cm high and the circular output aperture was 4.19 cm². A numerical consideration of the antechamber response to non-reactive incoming gases was conducted and the model results are presented in the calibration section to follow.

The antechamber also provided a means of achieving chemical equilibrium for the incoming gases via collisions of the gas particles with the antechamber surfaces. For example, atomic oxygen striking the chamber walls could recombine with adsorbed particles and eventually be re-emitted in the form of desorbed molecules. Note that although essentially all neutral gas particles measured by the cold cathode were chemically accommodated it was not possible to discern the chemical composition of the neutral flux from these measurements alone.

## 2.3  Magnetic Shielding

The PG sensor unit contained a significant magnet (having a magnetic dipole moment of approximately $10^4$ pole-cm). The external effects of the dipole were minimized by an arrangement of fixed compensation magnetics attached to the inside wall of the cylindrical sensor unit. Magnetic compensation was conducted at the JHU/APL in October 1988 by Mr. Fred Mobley. Calibrations conducted before and after magnetic compensation showed that the operation and sensitivity of the gauge were not measurably affected by the additional magnets. The effective dipole moment external to the IBSS PG sensor was 454 pole-cm.

## 3.  PRESSURE GAUGE CALIBRATION

The IBSS PG was calibrated by a series of vacuum chamber tests to measure both the steady-state accuracy and the temporal response of the gauge and numerically simulation of the response of the gauge antechamber. The vacuum chamber tests were conducted at the SenTran Company, the Johns Hopkins University Applied Physics Lab (JHU/APL), and the Air Force Geophysics Laboratory (now the Phillips Laboratory, Geophysics Directorate).

### 3.1  Steady-state PG Calibrations

Steady-state pressure calibrations for the IBSS PG were done by comparison to reference pressure gauges at each of the facilities noted above. Absolute pressure calibrations were difficult to achieve due to spatial variations in pressure at different locations within the test vacuum chambers and limitations on the availability of NBS (National Bureau of Standards) traceable standards over the full instrument range. The most extensive calibrations for the IBSS gauge were conducted at the JHU/APL on two separate occasions in May 1988 and January 1989. At these times the IBSS PG was calibrated against three separate reference gauges within the limited

6

pressure range from ~$10^{-6}$ Torr to several times $10^{-4}$ Torr. Dry $N_2$ at 1 ATM was introduced into the chamber to vary the pressure. The references used to calibrate the PG were; 1) a comparable Varian model 524-2 Cold-Cathode Gauge (unmodified), 2) a Bayard-Alpert hot cathode ion gauge, and 3) a nude gauge; that is a hot-filament gauge minus the glass enclosure. A systematic pre-shipment calibration was also conducted at the SenTran Company in May 1988. The SenTran Company calibrations were made using a reference gauge for the range from $10^{-7}$-to-$10^{-3}$ Torr and by simulation below $10^{-7}$ Torr. A notable difference for the SenTran calibrations was the removal of the antechamber for these tests. Periodic checks of the PG calibration were made at the Phillips Laboratory between January 1989 and October 1991 (post-flight).

Comparative calibration curves obtained during the JHU/APL and SenTran calibration tests are plotted in Figure 2. Mid-range comparisons from $10^{-7}$ to-$10^{-5}$ Torr were reasonably close and within a factor of 2. The deviations became more apparent at the extreme ranges of the instrument, varying by as much as a factor of 3. The adopted calibration equation for the IBSS PG was determined from a least-squares fit of the JHU/APL data and given as,

$$LOG_{10}(P) = 0.86 \ V_{TM} - 7.71 \qquad [1]$$

where $P$ is the measured pressure in Torr and $V_{TM}$ is the 0-to-5 V telemetry output voltage of the instrument. A semi-log plot of the adopted calibration curve in Eq. (1) is also included in Figure 2. Note that the pressure calibration performed at the SenTran Company gave consistently higher values of the accepted value for pressures above about $10^{-6}$ Torr. The periodic pressure checks made at the Phillips Laboratory are also included in the calibration plot for comparison.

The effects of gas composition on the IBSS PG calibration curve can be important. The JHU/APL calibrations of the IBSS PG were conducted using a $N_2$-dominated chamber environment. Variations in the pressure response of the gauge to different gases having masses close to that of $N_2$ are expected to be within about 10% [*Riddleford*, 1951]. A larger discrepancy in pressure of perhaps a factor of 8 is expected for $H_2$ due to the reduced sensitivity of the gauge to the lighter gases. This error has a possible bearing on thruster-induced pressure changes relative to the mass spectrometer observations of *Narcisi et al.* [1983; see also *Hunton*, 1994] showing that the dominant contaminant gas in the bay during operations of selected RCS thrusters was $H_2$.

The SenTran calibrations also included measurements of the temperature dependence of the PG within the operating temperature range of the instrument, -40 to +65 C. In all cases the
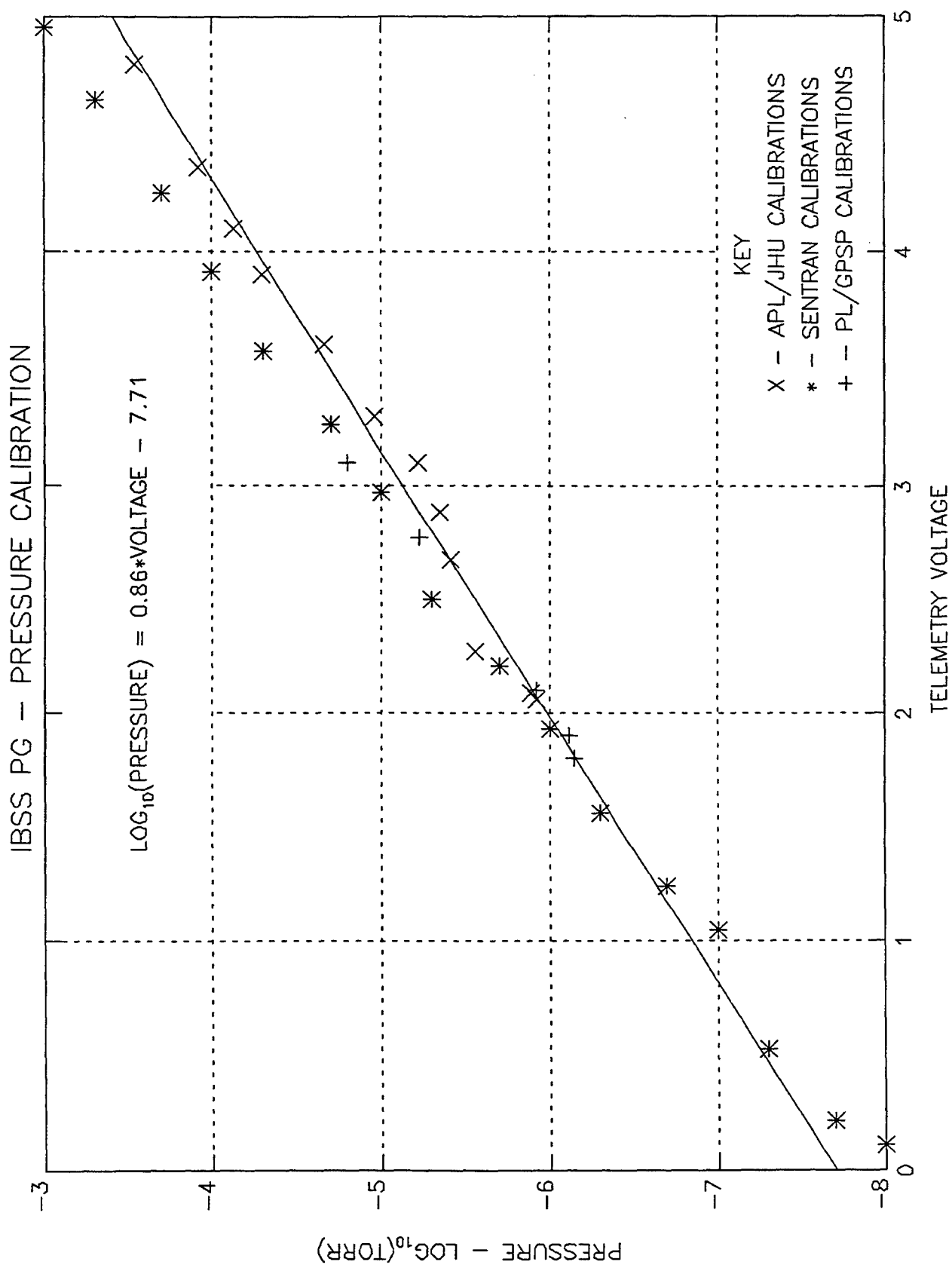
Figure 2. Calibration Curve for the IBSS Pressure Gauge

dependencies of the pressure measurements to temperature were well within the calibration errors noted above. Thus, no temperature corrections were included in the adopted calibration equation.

## 3.2    Numerical Modeling of the Antechamber

The spherical antechamber of the IBSS PG was designed to allow chemical and thermal accommodation of the incoming gases and to provide a tractable geometry for calculating the ram angle dependency of the measured pressure. Relative to this latter point, the steady-state and time-dependent responses of the PG were modeled via a simple kinematic approach for the motion of the particles within the antechamber. The geometry of the gauge antechamber for the model was similar to that shown in Figure 1 although the areas of the front and rear apertures were assumed to be the same and equal to 5.07 cm$^2$. Free molecular flow conditions within the antechamber were assumed since the scale sizes of the gauge system were much less than the collisional mean free path for pressures below 10$^{-3}$ Torr. At the aperture of the antechamber a statistical velocity distribution for the incoming gas particles was numerically generated and the particle motion within the chamber tracked. Two distinct gas populations were used in these simulations representing the extremes for the contaminant and atmospheric gas components. The contaminant gas was modeled as a Maxwellian distribution of particles having a 300 K temperature and characteristic of measured Shuttle surfaces. Atmospheric gases were represented as a flux of 1000 K particles incident on the gauge with a bulk speed of the spacecraft; that is, 7.4 km s$^{-1}$. Using this approach the antechamber throughput efficiency and temporal response for various flow conditions could be approximated.

The assumed Maxwellian distribution function for a thermally-distributed population of $m$-mass particles at temperature $T$ is

$$f(\underline{r},\underline{v})d^3rd^3v = n(m/2\pi kT)^{3/2}e^{-mv2/2kT}d^3rd^3v \qquad [2]$$

where $n$ is the gas density, $\underline{r}$ and $\underline{v}$ are the distribution's position and velocity vectors, and $k$ is Boltzmann's constant. According to the Equipartition Theorem of classical statistical mechanics, the probability of a particle having a component of velocity between $v$ and $v+dv$ is,

$$f(v)dv = (2\pi\sigma)^{-\frac{1}{2}}e^{-v2/2\sigma2}dv \qquad [3]$$

9

where $\sigma=\sqrt{kt/m}$. The total probability, $F(v_i)$, that a particle has a velocity component not exceeding $v_i$ is the integral of Eq.(3) over the component velocity space from negative infinity to $v_i$ as,

$$F(v_i) = (2\pi\sigma)^{-\frac{1}{2}}\int e^{-v2/2\sigma}dv \quad [4]$$

Equation (4) is the cumulative probability for a normal distribution [*Selby*, 1967]. This probability is linear from 0-to-1 for velocity components from negative-to-positive infinity, respectively. Equation (4) is solved for $v_i$ as,

$$v_i = \sqrt{2\sigma}\ erf^{-1}(2F\text{-}1) \quad [5]$$

where $erf^{-1}$ is the inverse error function. Thus, a Maxwellian distribution of particle velocity components could be simulated using Eq.(5) and a randomly generated set of $F$'s between 0 and 1.

Model simulations were initiated by introducing ensembles of randomly distributed particles at either the front or rear apertures of the gauge antechamber. Individual particle tracking indicated that, on average, incoming particles underwent multiple scattering on surfaces before exiting the antechamber. At each scattering surface new velocity components were generated, based on the temperature of the surface [*Harris*, 1991]. These scattered gas particles were then re-emitted from a rough surface (on molecular scales) according to a cosine probability curve of Lambert's Law of Emission. The temporal and steady-state responses of the antechamber were approximated by stepping the problem forward in time and monitoring the losses out of the antechamber. Continuity was achieved by re-introducing particles lost through the front and rear apertures. These newly-created particles had velocity components in accordance with the initial distributions.

### 3.3    Situation 1: A Maxwellian Distribution of Particles

Numerous modeling scenarios of the antechamber response and efficiency were made for Maxwellian particle distributions incident on the front and rear apertures. These distributions approximated situations resulting from sudden increases or decreases in the pressure external to the PG. Case 1 details the gauge response to an increased flux of particles at the front aperture. Particles lost through both the front and rear apertures were replaced at the front. The second example simulates the case of a sudden decrease in the external pressure or, equivalently

10

an enhanced particle flux at the rear aperture only. A constant "backpressure" was maintained by re-introducing at the rear antechamber particles which exited the problem. Case 3 examines these losses in somewhat more detail by re-introducing only those particles which exited the rear aperture while particles lost out the front aperture were not re-introduced. Finally, Case 4 mimics the situation of pressure balance at the rear antechamber by equalizing the flux lost and introduced at the rear antechamber. In each of the four examples the total number of particles under consideration was fixed and equal to the initial number of particles.

The temporal response of the antechamber to a 300 K distribution of 28 AMU neutrals ($N_2$) maintained at the front aperture of the gauge is shown in Figure 3a for Case 1. Within the figure the solid line corresponds to the percentage of incoming particles that scattered within the gauge and exited the front aperture. The dashed line is the percentage of particles that exited the rear and entered the cold cathode region of crossed $E$ and $B$ fields. This latter curve is referred to as the throughput efficiency of the gauge. The model calculations indicated that the response time of the system was initially quite rapid, being on the order of 1 to 2 ms with steady-state conditions reached after about 5 ms. The final throughput efficiency for the antechamber was determined to be about 11% with the bulk of the incident particles having been lost out the front aperture after undergoing about six collisions with internal gauge surfaces. Although an initial gas temperature of 300 K was assumed for the locally produced contamination, it was found that the steady-state gauge response was quite insensitive to temperature variations up through a tested level of 1000 K. This result was consistent with the incoming particles undergoing multiple scattering from surfaces within the antechamber and the assumption that the incident gases were rapidly thermalized to the gauge temperature.

The Case 2 results for a "backpressure" effect following a sudden decrease in external pressure are shown in Figure 3b. The assumed initial particle distribution was a 28 AMU, 300 K gas randomly distributed at the rear aperture of the antechamber system. As in Case 1, the solid and dashed curves correspond to particles lost out the front and rear apertures, respectively. Lost particles were continuously re-introduced at the rear antechamber with the thermal distribution of the initial gas. In this case it was assumed that the rear aperture was in contact with a reservoir at a higher pressure than the front. The model results indicated that the temporal response of the gauge, subjected to a backpressure effect, was comparable to that of Case 1. On the other hand, the throughput efficiency for this case was quite distinct. Specifically, particles introduced at the rear aperture of the antechamber had only a 37% probability of exiting the front (solid curve) whereas the probability that particles were back-scattered into the cold cathode was 63% (dashed curve).

11

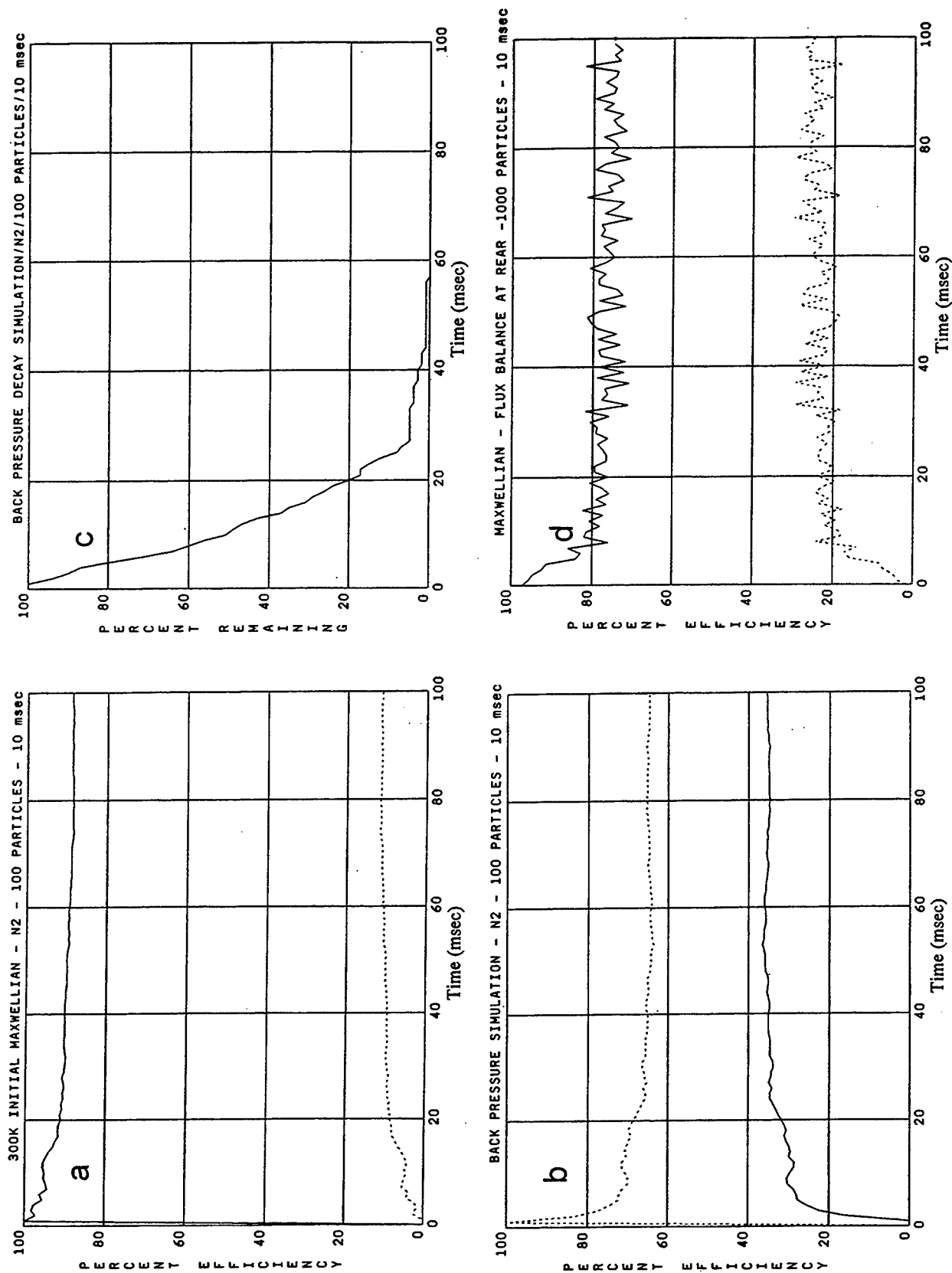Figure 3. Simulation Results of the Pressure Gauge Antechamber for a Maxwellian Distribution of 28 AMU and 300 K Neutral Gas Particles for Four Separate Cases as Noted. The dashed (solid) curve in plots *a*, *b*, and *d* refer to the percentage of particles that exit the problem through the entrance aperture. The curve in plot *c* is the percentage of active particles remaining in the problem and not having exited the front aperture

Case 3 also models the gauge response to a sudden decrease in pressure external to the gauge. This differed from Case 2 in that particles exiting the front were permanently lost to the problem; that is, their particle motions were stopped. On the other hand particles exiting the rear antechamber were re-introduced at the rear interface. The results of the simulation are plotted in Figure 3c. These results simulate the realistic case of a finite volume of gas which must evacuate the interior of the gauge. The plotted curve in Figure 3c represents remaining in the simulation vs time. The result of this model indicate that the temporal response of the gauge to evacuate the cold cathode following a sudden decrease in external pressure was on the order of several milliseconds, as expected.

The final case illustrates the situation where the net flux of particles crossing each interface; that is, the front and rear apertures, is equal to zero. The initial distribution was assumed unbalanced with the only source of particles being a 300 K gas incident on the front aperture. Thereafter, particles lost out the front and rear of the antechamber were reintroduced at their respective apertures. The model continued until there was a steady-state balance between the number of particles leaving the antechamber through each aperture. Figure 3d is a plot of the percentages of particles exiting and entering the front (solid curve) and rear (dashed curve) apertures of the PG antechamber. These results indicate that the time required for the system to reach steady-state is on the order of several milliseconds with the most rapid changes occurring within the first millisecond.

Figure 3d also shows that on average the flux of particles passing in each direction through the front aperture was about four times greater than the corresponding number at the rear. These results are seemingly in disagreement with the expectations of gas dynamics which would tend to equalize the thermal flux of particles passing through any aperture in a steady state system. However, it should be recalled that the model assumed free molecular flow within the gauge and that the geometry of the antechamber was a determining factor responsible for this ratio. Pressure balance was not an integral part of the analysis and systematic variations in the model and measurements are not unexpected. For example, based on this analysis there was a 4-to-1 difference in the number density of particles near the front and rear apertures. While this indication of an enhanced number density is of interest, it is important to bear in mind that the instrument calibration at APL/JHU was derived from comparative data using the fully assembled PG and laboratory standards. This trend was consistent with the larger than anticipated pressures (see Figure 2) for the SenTran calibrations, which were conducted without the antechamber in place.

An additional factor is the model assumption that gases within the antechamber and the cold cathode were inert. In reality, adsorbed ions on internal gauge surfaces were potential

13

sources of desorbed neutral gases which had access to the antechamber via the rear aperture. These desorbed gases operated on time scales quite independent of the model results which were based on geometric considerations alone. In spite of this uncertainty, the above calculations were useful to the understanding of the gauge geometry and for determining the minimum temporal response of the PG. Thus the modeled response time for the PG, found to be on order of several milliseconds, should be considered a minimum.

## 3.4 Situation 2: A Drifting Maxwellian Gas

A conceptually similar appproach was used to determine the PG response to atmospheric gases flowing relative to the spacecraft. Distinctly different however, was the form of the initial particle distribution used, which was a drifting Maxwellian in the present case. In this simulation, gas particles were randomly distributed on the entrance aperture of the antechamber. The bulk flow of the incoming atmospheric gas was assumed to be 7.4 km s$^{-1}$ directed at some fixed angle relative to the gauge aperture normal. As in the previous case, it was assumed that incoming particles multiply scattered within the chamber and became rapidly thermalized to the temperature of the gauge. Thus, the individual particle motions within the antechamber following the first scattering collision were similar to the cases involving an initial, non-drifting Maxwellian distribution.

The model results for the PG response to atmospheric gases is shown in Figure 4. These results indicate that the throughput efficiency (dashed line) of the antechamber was dependent upon the angle of the incoming gases relative to the aperture normal. The variation in the efficiency was between 4% for normal incidence at 0° and a maximum of 18% near 30°. The top solid curve in Figure 4 is the percentage of particles that exited the problem through the entrance aperture. The lower solid curve is the average number of collisions made by the incoming particles within the antichamber before exiting the problem. The lower throughput efficiency near 0° was a consequence of the fewer collisions, on average, that a particle made before exiting the problem compared to particles entering at larger input angles. Closer to perpendicular incidence, that is near 90°, the throughput efficiency of the gauge was about 9% and similar to the model results for a non-drifting initial distribution (see Figure 3a). An additional finding (not shown) was that the temporal response of the gauge over all incidence angles was on the order of several milliseconds.

Note that under steady state conditions a balance existed between the incoming and outgoing particle fluxes through the gauge entrance aperture. Of course, the bulk speed of the atmospheric population entering the gauge was greater than the thermal speed of the exiting gas.

14
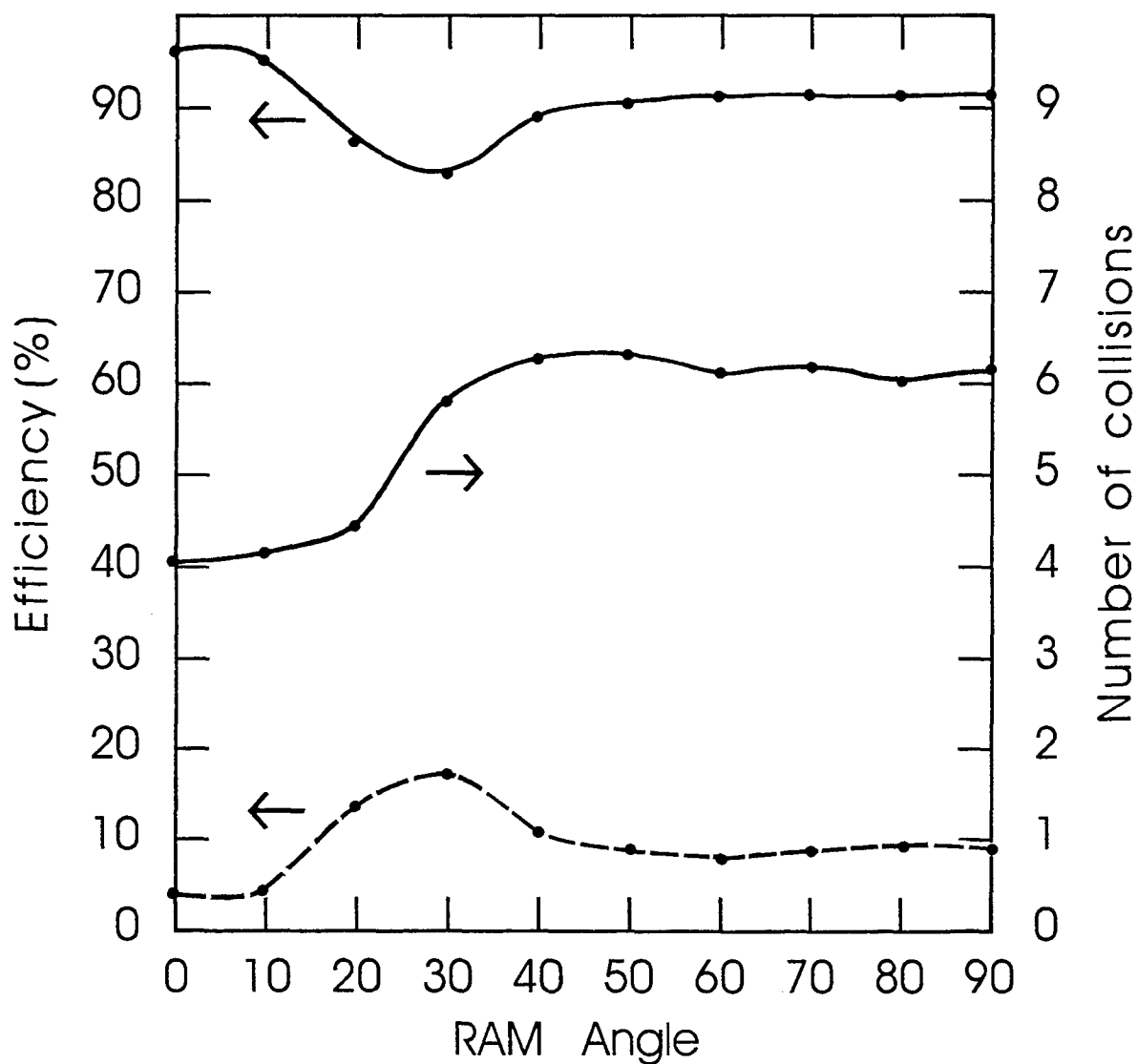
Figure 4. PG Antechamber Efficiency vs Angle for Ram-flowing Gases. The gauge aperture normal is oriented into the ram at 0°. The dashed curve shows the throughput efficiency, whereas the top solid curve is the percentage of particles that exit the problem through the entrance aperture. The lower solid curve is the average number of collisions made by the incoming particles within the antechamber before exiting the problem. This simulation involved 100 active particles for 10 ms

This required that the particle density and, in turn, the pressure within the antechamber be larger than the external atmospheric pressure. As will be shown latter, this requirement of flux balance was used to estimate the atmospheric pressure during the STS-39 mission. However, the angular dependence in the modeled throughput efficiency of the gauge, particularly at normal incidence, implies that the assumption of thermal equilibrium may be violated for cases where the incoming particles undergo fewer scattering collisions from gauge surfaces.

## 4. DATA PRESENTATION AND DISCUSSION

Survey plots of the IBSS PG measurements for STS-39 are provided in Figure 5 and a general list of relevant events and times is contained in Table 1. Unless otherwise noted, all times are referenced to Mission Elapsed Time (MET) for a Shuttle launch that occurred at 1133 GMT on 28 April 1991. This section is divided into several subsections that cover the overall pressure profiles for the mission, measurements for the in-bay and deployed phases, the effects of controlled gas releases from engines and other sources, and pressure variations due to attitude changes.

### 4.1 Geometric considerations for the IBSS PG on STS-39

The IBSS PG for STS-39 was mounted on the Shuttle PAllet Satellite (SPAS) carrier and oriented such that the aperture normal of the gauge was aligned with the boresights of the Low Light Level TeleVision ($L^3TV$) cameras and the infrared radiometer/spectrometer. The placement of the PG on a side plate of the SPAS is shown in Figure 6 along with the coordinate definition of the $L^3TV$ system. Note that in the $L^3TV$ coordinate system the optical instruments and the PG were aligned with the positive-$X$ axis, the positive-$Z$ axis pointed down towards the SPAS keel trunnion, and the $Y$-axis completed the right-handed system. At times during the mission the SPAS positive-$X$ was oriented in the ram direction causing the PG to sample a direct flux of atmospheric gases into the gauge. Also indicated in Figure 6 are the locations of the Attitude Control System (ACS) $N_2$ thrusters, indicated as ACS 1 to 3, which were used for SPAS maneuvering while the payload was deployed.

Within the Shuttle, the SPAS was located approximately halfway back in the cargo bay as indicated in Figure 7. Also shown in the figure are the locations of the AFP-675 (SKIRT) and STP-1 (CIRRIS) payloads as well as the instruments for the separate Chemical Release Observation

16
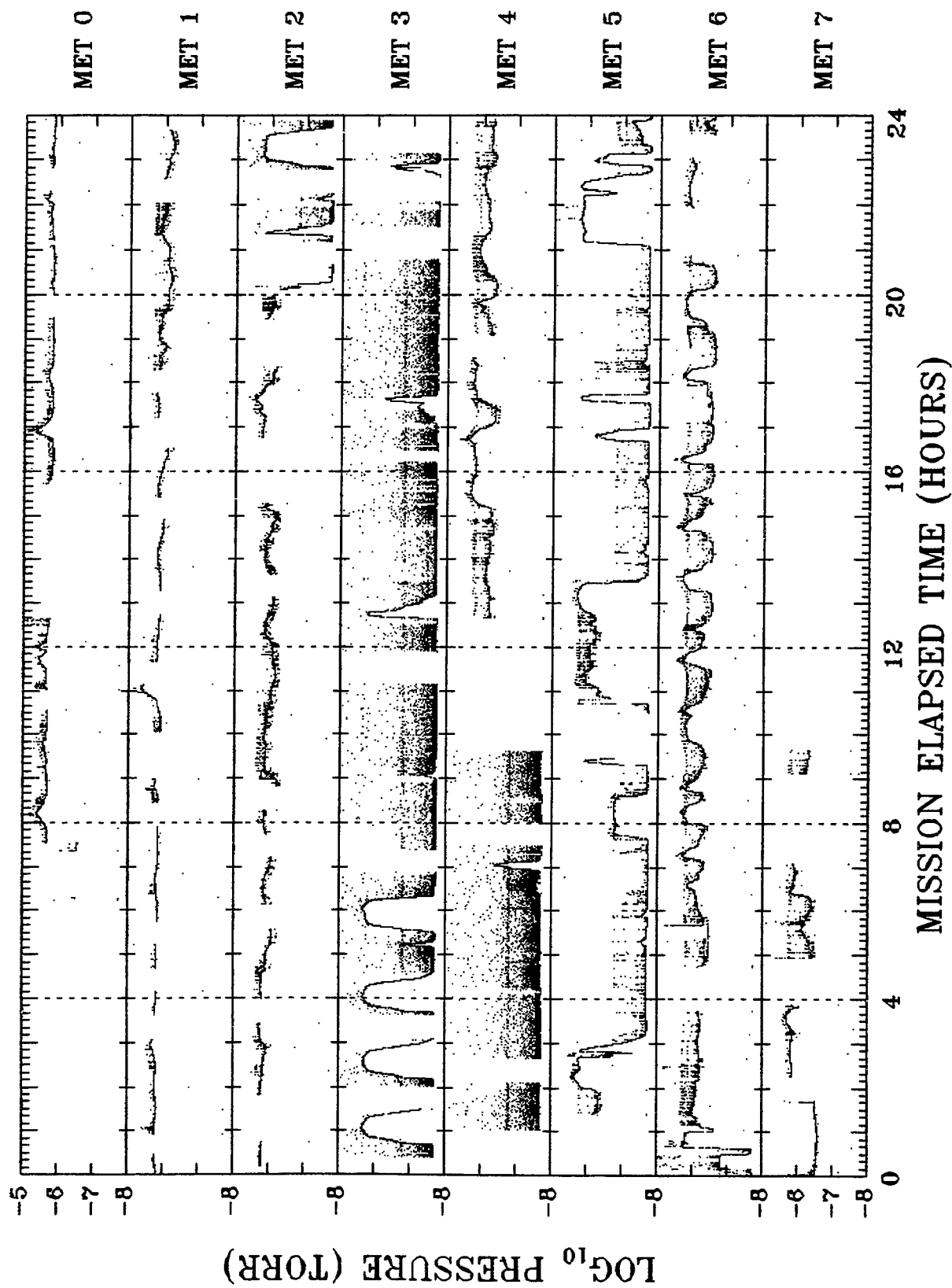
Figure 5. Survey Plot of the Measured Gas Pressure: Within the Shuttle Bay, On the Remote Manipulator System, And As a Deployed Subsatellite for Mission STS-39. Refer to Table 1 for the Event History for STS-39

17

Table 1. Event History for the STS-39

| MET | Event | Comment |
|-----|-------|---------|
| 0/00:00 | Launch | Start of mission at 118/11:33:07 GMT |
| 0/01:26:57 | Doors open | Payload bay doors open |
| 0/07:20:35 | PG ON | PG turned on |
| 2/16:50:00 | SPAS Unberth | Start of RMS operations |
| 2/20:44:38 | SPAS Release | SPAS freeflyer from 02/20:44 to 4/11:36 |
| 4/10:52:20 | SPAS Capture | SPAS attached to deployed RMS |
| 4/11:36 | SPAS Berth | SPAS returned to payload bay |
| 5/02:32:22 | SPAS Unberth | RMS operations - SPAS attached to RMS |
| 5/10:43 | SPAS Berth | SPAS returned to payload bay |
| 5/13:30 | SPAS Unberth | RMS operations - SPAS attached to RMS |
| 6/01:08:46 | SPAS Berth | SPAS returned to payload bay |
| 7/09:40 | PG OFF | PG turned off |
| 8/04:35:20 | Doors closed | Payload bay doors closed |
| 8/07:23:24 | Landing | Shuttle stopped on ground |

(CRO) and Critical Ionization Velocity (CIV) experiments that were considered part of the IBSS mission payload. Note that during bay operations the PG on the SPAS was below the sill of the cargo bay and "looked" into the inner starboard wall of the Shuttle. At no time while in the cargo bay did the PG view free space. The relevant coordinate system for cargo bay operations was the Orbiter body axes, as shown, with the negative-$Z$ axis pointing directly upward out of the payload bay and positive-$Y$ towards the starboard. The definitions for sequential Yaw-Pitch-Roll maneuvers are also indicated.
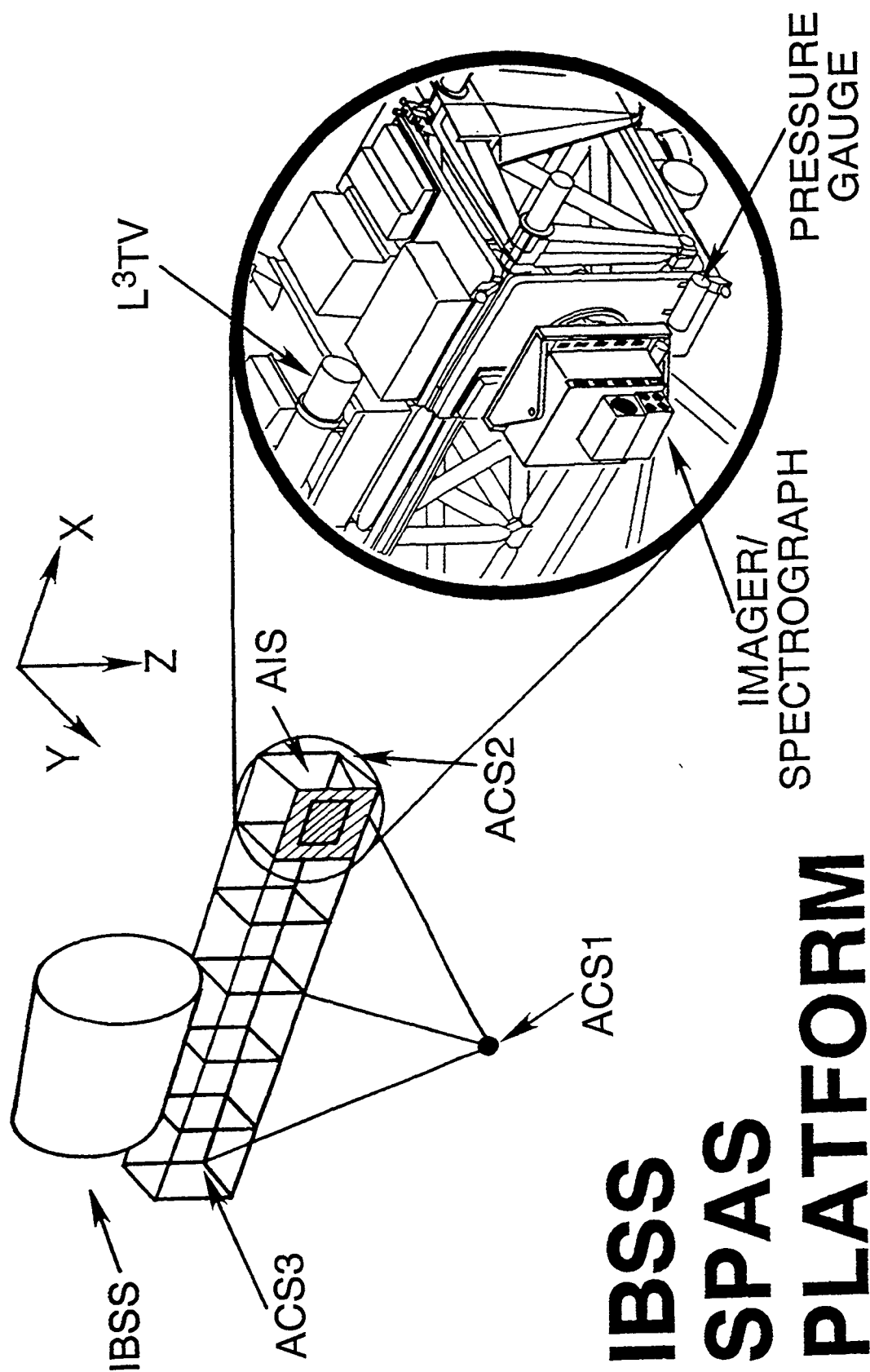
IBSS
SPAS
PLATFORM

Figure 6. Location and geometry of the PG on the IBSS SPAS relative to the AIS Imager/Spectrograph and the L³TV. The locations for the three SPAS attitude control thruster assemblies, ACS 1, 2, and 3 are also indicated. The L³TV coordinate system is defined in the upper center
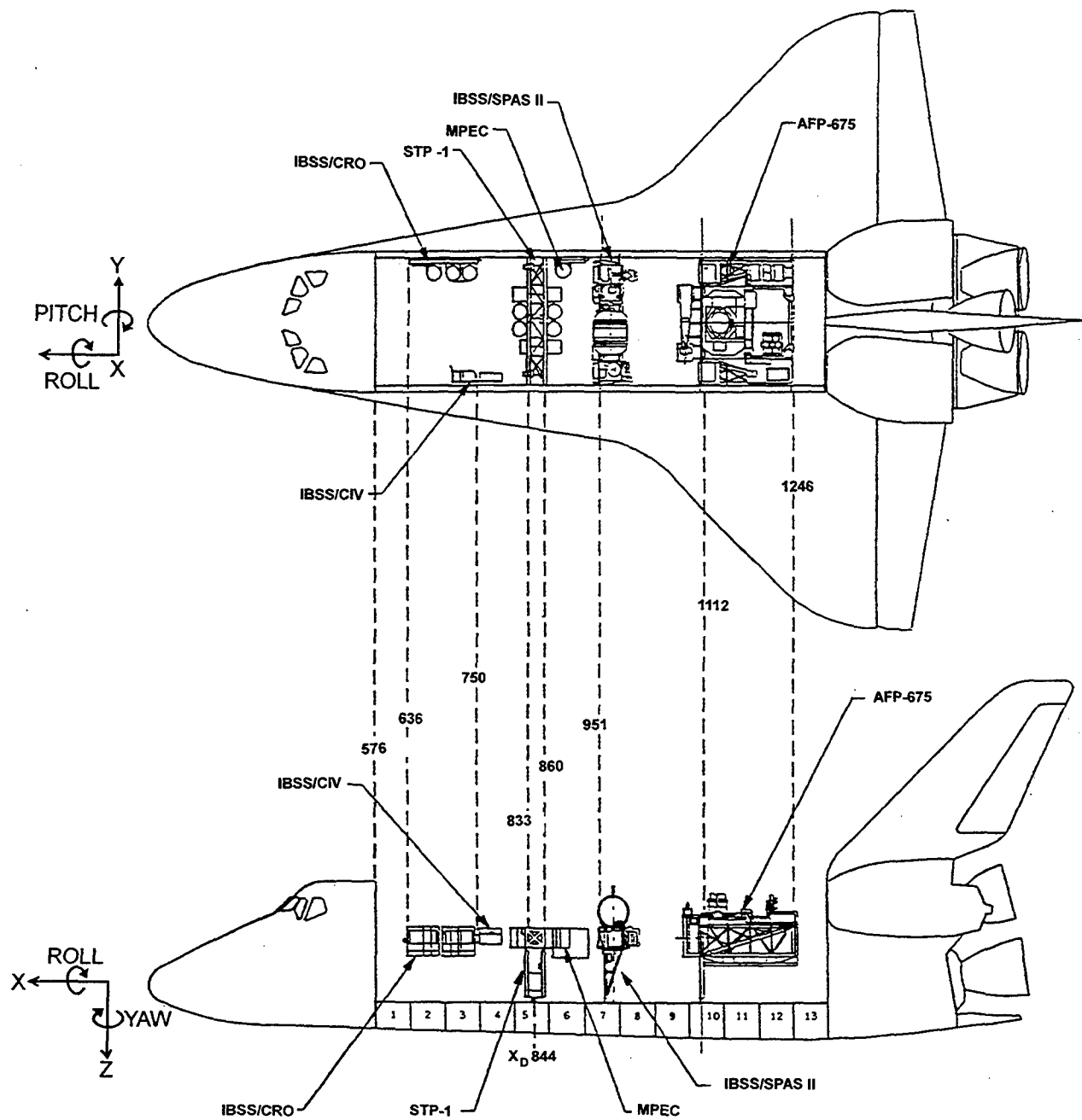
Figure 7. Location of the IBSS SPAS within the Shuttle's cargo bay. The Orbiter body axis coordinate system is shown along with the definitions for the yaw, pitch, and roll maneuvers. Note the locations of the AFP-675 (CIRRIS) and STP-1 (SKIRT) payloads and of the associated CRO and CIV instruments.

## 4.2    Overall Mission Pressure Survey

IBSS PG neutral gas measurements for mission STS-39, plotted in survey form in Figure 5, indicate that the pressure profile for the mission was highly variable and changed by orders of magnitude throughout the flight. These variations were due to changes in the attitudes of the Shuttle and the SPAS, operations of reaction control jets and other gas releases and, at times, instrumental effects. The PG was turned on approximately 7 hours after launch and several hours after the payload bay doors were opened and the cargo bay evacuated. Thereafter the gauge operated almost continuously until the end of the IBSS experiment on MET day 7 although there were numerous telemetry drop-outs and blackout periods (no telemetry available) that occurred throughout the mission, causing losses of PG data. Several times during the mission the SPAS was removed from the cargo bay for extended operations while attached to the Remote Manipulator System (RMS). The SPAS was also deployed as a subsatellite for an extended period between 2/2044 and 4/1136 MET. During the deployed interval the maximum separation distance between the Orbiter and the SPAS was 17 km although for the most part the SPAS was stationed at about 10 km from the Shuttle. Minimum separation for deployed operations was 2.2 km.

The PG summary plots show that the baseline pressure measured within the bay decreased from about $2 \times 10^{-6}$ Torr on MET day 0 to several times $10^{-7}$ Torr on day 7. The rate at which the baseline pressure decreased conformed roughly to that of an exponential with a decay time of about 2.5 days. Superimposed on this baseline were two general classes of pressure variations, distinguished by their respective time scales. Systematic variations in pressure, having periods on the order of 1 to 2 hours, appeared to have been the result of orbital attitude changes. On the other hand, the transient pressure spikes having the appearance of noisy data were the result of attitude control jet firings and other controlled gas releases. Similar variations, both systematic and transient, were also measured while the SPAS was outside the payload bay either on the RMS or deployed as a free flyer. However the RMS and deployed-SPAS measurements were distinct from bay operations in that the PG had an opportunity to "view" free-space. While the SPAS was deployed the pressure within the gauge antechamber was often below the sensitivity threshold of the PG, as indicated by a minimum baseline pressure of $2 \times 10^{-8}$ Torr (see Figure 2).

The IBSS PG measurements indicate that the baseline pressure profile within the payload bay was significantly above the atmospheric background level throughout the STS-39 mission. The rapid decrease in the measured pressure during the deployed phase shows that the elevated bay pressures were real and not related to outgassing within the gauge itself. On the other hand,

the steadily decreasing pressures throughout the mission indicate that the local contamination was from outgassing sources within the payload bay rather than from a steady-state source such as leaking from the pressurized crew cabin or nearby cryostats. Such sustained high pressures within the payload bay do not agree with NASA specifications [Nicholson, 1988]. As noted earlier, Shawhan and Murphy [1983] found that on mission STS-3, in March 1982, the pressure within the exposed cargo bay dropped from $10^{-5}$ Torr several hours after launch to near background atmospheric levels within 24 hours. However the measurements from STS-39 were consistent with the observations of Kawashima et al. [1985] of a higher than expected pressure throughout the SpaceLab 1 mission.

The IBSS PG results for the systematic variations attributed to vehicle attitude changes and to the transient effects from controlled gas releases are considered separately. Although the in-bay measurements are representative of the in-situ gas fluxes to the PG antechamber and perhaps indicative of particle fluxes within the bay we caution that the location and orientation of the gauge were likely determining factors in the instrument's pressure response during this mission. On the other hand, data from the deployed portion of the mission provided an opportunity for ram-to-wake pressure comparisons. Similarly the responses of the gauge to the separate attitude control systems for the Shuttle and the SPAS were distinct. Other potential sources of local gas pressure perturbations were from OMS engine firings, water dumps and flash evaporators, and the associated CRO and CIV experiments.

## 4.3    Anomalous Pressure Gauge Operations

The initial PG measurements for STS-39 are shown in Figure 8a for the interval between 0/0700 and 0/0800 MET. This figure also includes a record of the RCS thruster firings, indicated by short vertical lines for each thruster (left ordinate). The overall effect of these thruster firings will be discussed in subsequent sections. Immediately following gauge turn-on at 0/0720 MET the gauge reading was anomalously low, possibly because the cathode was contaminated. Such contamination limited the available conducting surface area of the gauge and resulted in reduced current flows within the cold-cathode gauge [G. Murphy, private communication, 1991]. After several minutes of operation the cathode surface became "conditioned" and the subsequent pressure readings were more characteristic of payload bay measurements from previous Shuttle missions [Pickett et al., 1985]. Thereafter and periodically throughout the flight the pressure record indicated short-lived intervals, on the order of several seconds to tens of seconds during which time the measured pressure was slightly less than the baseline.

IBSS PRESSURE GAUGE – MISSION DAY 0



IBSS PRESSURE GAUGE – MISSION DAY 6
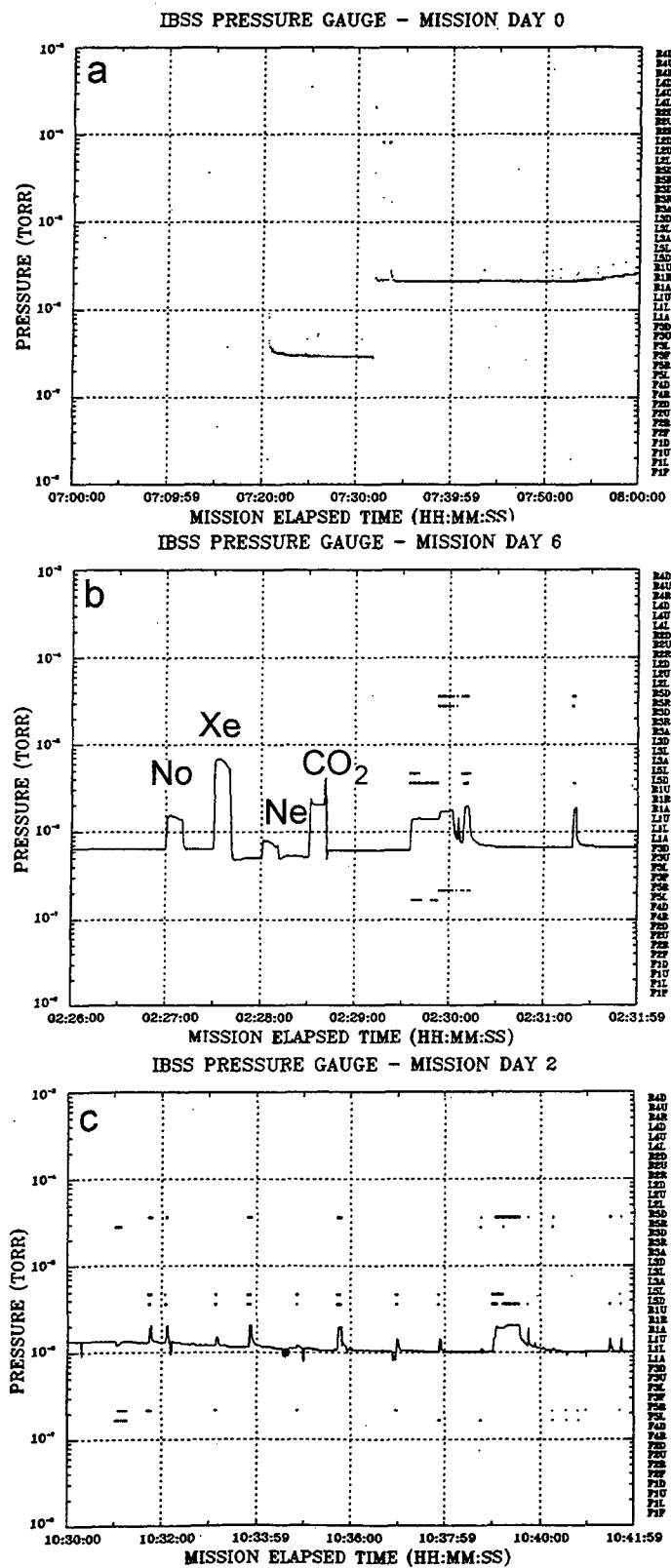


IBSS PRESSURE GAUGE – MISSION DAY 2



Figure 8. Sample Data Plots of Anomalous Gauge Behavior for: a) Initial PG Operations Showing an Unexpectedly Low Pressure Reading Early in the Mission and a Step-like Pressure Change, b) Step-like Offset in Pressure During the CIV5 Gas Release Sequence for Xe, and c) Apparent Short-lived Pressure Uncorrelated with Known Thruster Firings

23

A similar loss of sensitivity occurred at the time of the controlled release of xenon gas during one CIV sequence. The relevant data are shown in Figure 8b for the set of four gas releases that comprised this CIV sequence. The CIV experiment consisted of the sequential release of nitric oxide (NO), xenon (Xe), neon (Ne) and carbon dioxide ($CO_2$). The total time duration of the plot is 6 minutes. It is apparent from a consideration of these measurements that during the Xe gas release the baseline pressure decreased 15 to 20% from just over $6\times10^{-7}$ Torr. The measured pressure returned to the higher baseline value about a minute later and just after the final gas release in this sequence. As an aside, note the relationship between the RCS thruster firings and the observed pressure.

Finally, clear examples of these short-lived drop-outs are also visible in the survey plot of Figure 5 during most of MET day 2. A 12-minute interval of data from MET day 2 is detailed in Figure 8c. Again, the figure is a comprehensive plot of the pressure and RCS engine firings - a subject covered in more detail later. However, note that the transient pressure depletions were not clearly correlated with any RCS engine firings. On the other hand, note further that the transient loss of sensitivity does not appreciably detract from the overall pressure measurement.

Such anomalous behavior has been noted in the operation of cold cathode gauges in space [*Goerke et al.*, 1992]. Unfortunately a detailed understanding of the causes for this loss of sensitivity is not available. However, this phenomena affected only a relatively small amount of the PG data for mission STS-39. Otherwise, the overall pressure record was well behaved throughout the entire Shuttle mission and consistent with known changes in the local gas environment.

## 4.4 Local Pressure Changes Due to Ram Angle Variations

Pressures measured throughout the mission had clear variations related to the orientations of the Shuttle and the SPAS to their respective velocity vectors. Such variations are evident in the composite pressure and RAM angle plots for MET days 3 and 6 presented in Figures 9a and 9b, respectively. These data correspond to pressure measurements made while the SPAS was deployed as a free-flyer on day 3 and located within the payload bay for most of day 6. The reference coordinates are the previously described Orbiter body axes for in-bay measurements and the $L^3TV$ coordinate system for deployed operations. An obvious difference between the measured pressures for these distinct configurations was the amplitudes of the systematic variations with in-bay pressures changing by a factor of 10 and the SPAS pressures varying by at least two orders of magnitude. Pressure measurements for in-bay and SPAS operations are discussed separately.
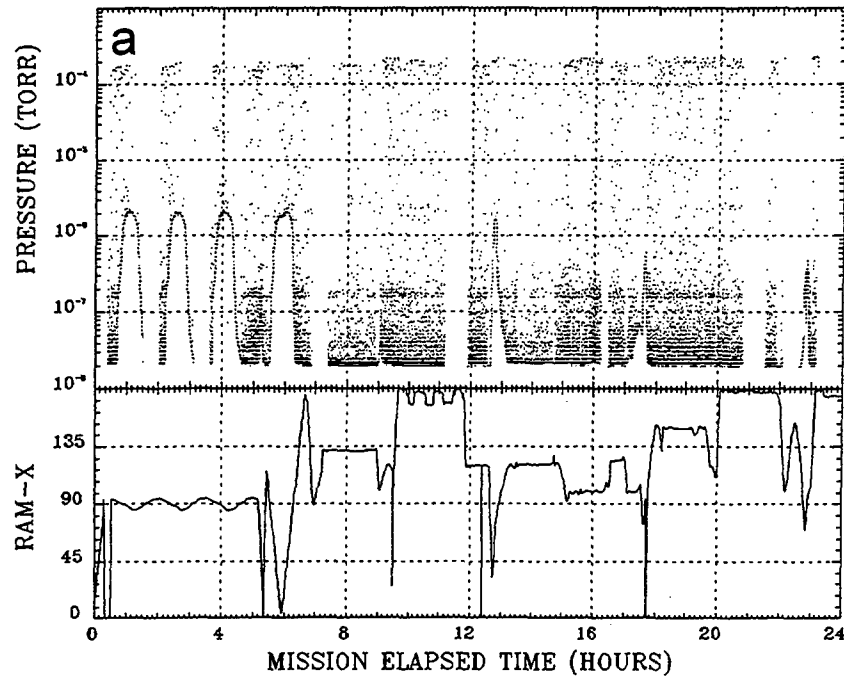
Figure 9. Plots of Pressure and Ram Angle Variations for: a) MET Day 3 While the SPAS Was Deployed as a Free-Flyer and b) MET Day 6 Within the Shuttle's Cargo Bay

25

## 4.5    SPAS Attitude Dependence of the Measured Pressure

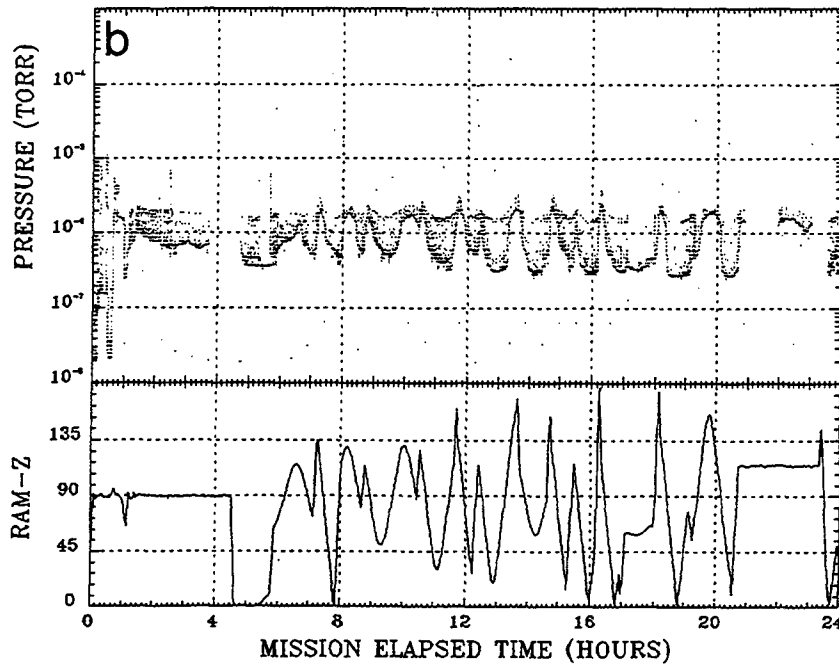The SPAS measurements for MET day 3, shown in Figure 5, indicate that the steady-state background pressure varied between $2\times10^{-6}$ Torr and the minimum instrument sensitivity of $2\times10^{-8}$ Torr. During the first few hours of the mission day the pressure had a well defined temporal variation that persisted until just after 0600 MET. Unfortunately these early times also corresponded to the interval of initial SPAS operations when the attitude of the SPAS was unconfirmed due to the failure of a sun sensor. Initial "strap-down" of the SPAS gyros occurred at 0520 MET and the attitude was finally confirmed at about 0700 MET. Subsequent to attitude confirmation, the peak background pressures were observed to be well correlated with the gauge aperture being directed towards the ram direction; that is, ram-$X$ angles less than 90°. This trend is can be seen in the composite plots of Figure 9a for 1244, 1737, and 2251 MET.

An operational constraint for the IBSS mission was the avoidance of atmospheric ram gas flow into the infrared radiometer/spectrometer. The aperture of the radiometer/spectrometer was co-aligned with that of the PG. Because of this restriction the aperture of the PG was only briefly exposed to the ram flowing gases after final attitude confirmation. However, while the PG aperture was exposed to the ram, the measured pressures were well above the baseline and on the order of $2\times10^{-6}$ Torr. On the other hand, during the initial deployment of the SPAS the pressure variations were more regular as evidenced by the distinct cyclic variations of the measured pressure. For example, the first three cycles of increased pressure on day 3 were equally spaced and phased with the Shuttle orbital period of 90 minutes. Thus the PG data suggests that during this interval the apertures of the PG and of the radiometer/spectrometer were exposed to ram gases for a significant fraction of the time. In addition, following the initial strap-down but prior to attitude confirmation the gauge aperture apparently swept through the ram with a cos-$X$ dependency consistent with subsequent measurements. The fact that SPAS was in an inertial hold configuration during this time is consistent with the orbital period of the pressure variations. As an aside, we note that the data dropouts that occurred around the time of the lowest measured pressures prior to 0400 MET may have corresponded to attitudes in which the SPAS antenna link to the Shuttle was unavailable due to geometric constraints.

The ram angle dependence in pressure for the time interval, 0600-to-0800 MET, is plotted in more detail in Figure 10. Also plotted is a normalized cosine curve showing the anticipated pressure response of the PG to changing ram angles. This cosine function relates the aperture area to the input angle and does not consider the efficiency of the gauge. The model results for ram-flowing gases show that in practice the efficiency of the antechamber was dependent upon
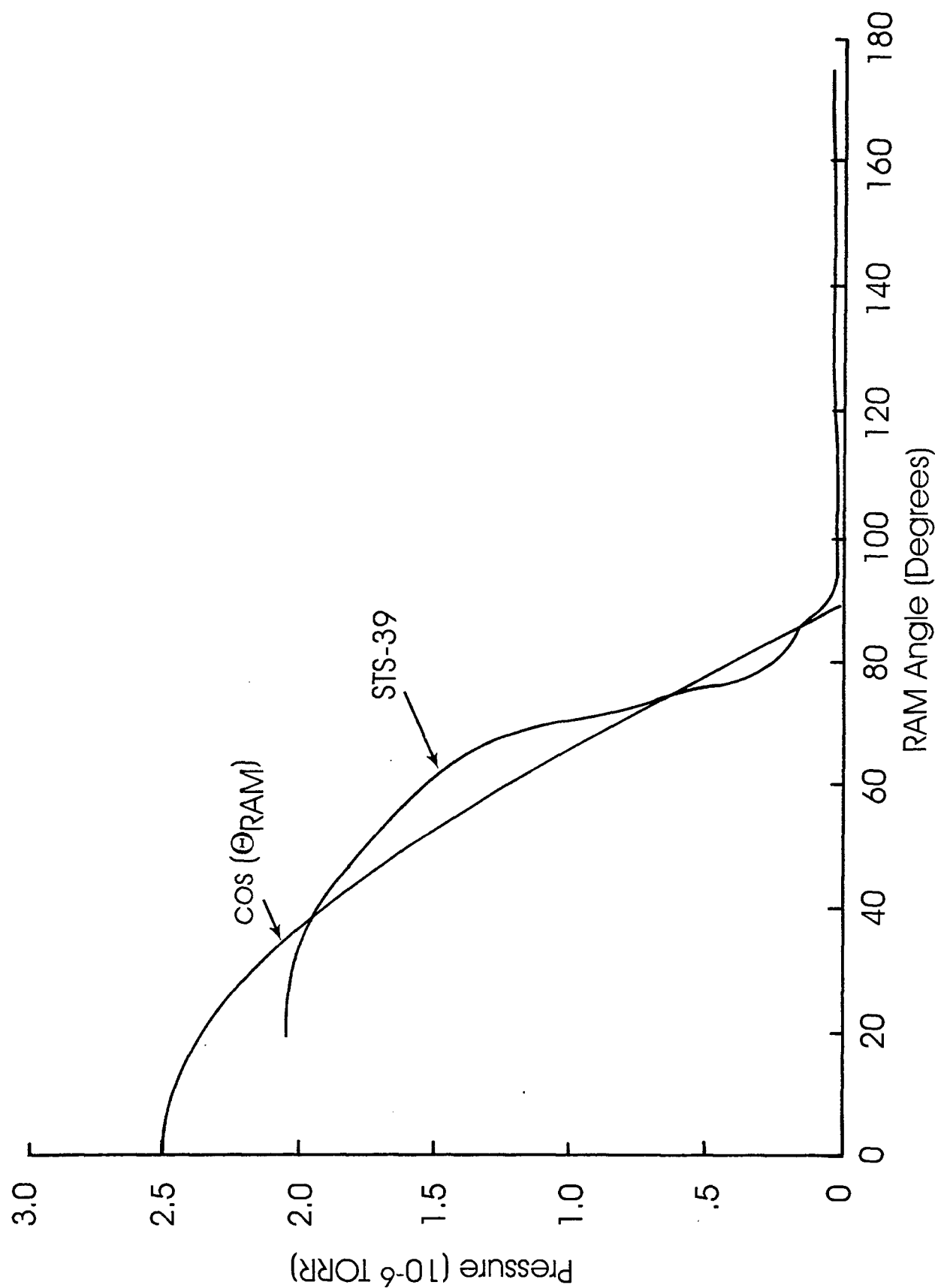
Figure 10. Plot of Pressure Versus Ram Angle Measurements While the SPAS Was Deployed. Pressure Data were obtained from Day 3; 0600-0800 MET. A normalized cosine curve is included in the plot for reference purposes

the input angle (see Figure 4). The flattening of the pressure curve at ram angles less than about 30° is consistent with the decrease in the gauge efficiency. However, the overall agreement between the data and model curves shows that the design of the antechamber achieved the desired result of a gauge system having a well behaved ram angle pressure response.

The gauge antechamber was designed to facilitate atmospheric gas density calculations. Under steady-state conditions the pressures within the antechamber and the cold-cathode gauge were assumed to be in equilibrium. Similarly, the fluxes of gases entering and exiting the aperture were equivalent in steady-state; that is, $F_{in} = F_{out}$. The maximum pressure for the ram-directed measurements was $2 \times 10^{-6}$ Torr. The principal contributor to the incoming flux was the atmospheric gases ramming into the gauge aperture. The directed speed with which these particles entered the antechamber was the 7.7 km s$^{-1}$ orbital speed of the SPAS, neglecting contributions due to random thermal motions. Background contamination due to surface outgassing of the SPAS and the transient effects of the reaction control jets were of minor importance to the measured steady-state pressure. Within the antechamber the high-velocity atmospheric particles underwent multiple scattering from the stainless steel chamber walls and were rapidly thermalized to the temperature of the surfaces; that is, approximately 300 °C. Thus the exiting neutral particles had thermal speeds of order 0.5 km s$^{-1}$. The equivalence between the incoming and outgoing fluxes in the steady state suggests the relationship,

$$n_a v_a \sim n_g v_{th} \qquad [6]$$

where $v_a$ and $v_{th}$ were the respective orbital and thermal speeds, $n_g = 6 \times 10^{16}$ m$^{-3}$ was the particle density within the gauge at the maximum pressure of $2 \times 10^{-6}$ Torr, and $n_a$ was the atmospheric density. Thus, the calculated value for the atmospheric density and pressure were $4 \times 10^{15}$ m$^{-3}$ and $4 \times 10^{-7}$ Torr, respectively, at an assumed atmospheric temperature of 1000 K.

The nominal atmospheric density at 260 km is $1.5 \times 10^{15}$ m$^{-3}$, consisting mostly of O (76%), $N_2$ (22%), and $O_2$ (1%) [*Dubin et al.*, 1976]. The calculated value for the density as determined from the analysis presented above was about a factor of 3 greater than this standard density. Recombination of the highly reactive atomic oxygen gas within the gauge antechamber may actually increase this apparent discrepancy. Relevant to the STS-39 measurements, however, we note that this Shuttle flight occurred just after solar maximum and during an interval of increased geomagnetic and solar activity. Under such conditions the thermospheric density at 260 km can increase by as much as a factor of 4.5. Thus, the atmospheric densities measured on SPAS while the PG was oriented towards the ram were well within the expectations of the U.S. Standard Atmosphere, 1976 [*Dubin et al.*, 1976].

28

## 4.6    Shuttle In-bay Operations

A general observation made earlier was that the in-bay pressures generally decreased throughout the 8-day mission. However, systematic pressure variations that were related to the attitude of the Orbiter also occurred within the bay. Figure 8b demonstrates that the relationship between the in-bay pressures and the ram-$Z$ coordinate was one in which the highest pressures were measured while the payload bay was facing into the ram; that is, ram-$Z$ angles greater than 90°. Conversely, the lowest pressures were measured while the payload bay was directed into the wake.

As noted earlier the PG was positioned within the bay so that the gauge aperture never sampled the direct atmospheric flux component. Rather, the gauge continuously "looked" into a starboard wall and below the sill of the payload bay. The peak pressures measured in the ram were therefore more representative of the flux of atmospheric gases scattered within the cargo bay or undergoing chemical processes such as absorption and desorption by Shuttle surfaces. Peak pressures within the cargo bay after MET day 0 remained about $10^{-6}$ Torr, consistent with a steady atmospheric contribution. On the other hand, PG measurements within the wake corresponded to the flux of particles from the continuous outgassing of the Shuttle and payload materials or desorbed gases. The wake pressures generally decreased throughout the mission with an exponential decay time of 2.5 days, as noted earlier. Thus the depth of the ram-to-wake variations increased throughout the mission due to the general decrease in the rate of vehicle outgassing.

It is also interesting to note in Figures 9a and 9b that the peak payload bay pressures that occurred while the bay was oriented towards the ram were comparable to the largest pressures measured during deployed operations while the gauge aperture was towards ram. This suggests that the simplicity of the gauge antechamber and the geometric complexity of the Shuttle bay payload were equally effective in multiply scattering atmospheric gas particles.

## 4.7    Pressure Decrease During RMS Operations and the SPAS Release

Early RMS operations of the SPAS payload provided an opportunity for a quantitative assessment of the PG pressure response as the SPAS was moved in close proximity to the Shuttle's cargo bay. During these operations, the PG measured changes in pressure as the SPAS was lifted out of the Shuttle cargo bay, held in a fixed position slightly above the sill of the payload bay, and then rotated by 90° so that the PG eventually viewed along the -$Z$ axis; that is, directly away from the cargo bay. The SPAS was subsequently released and the Shuttle then moved away from the free-flying SPAS. Figure 11 is a plot of the measured pressure during the period from 2/1930 to 2030

# IBSS PRESSURE GAUGE – MISSION DAY 2
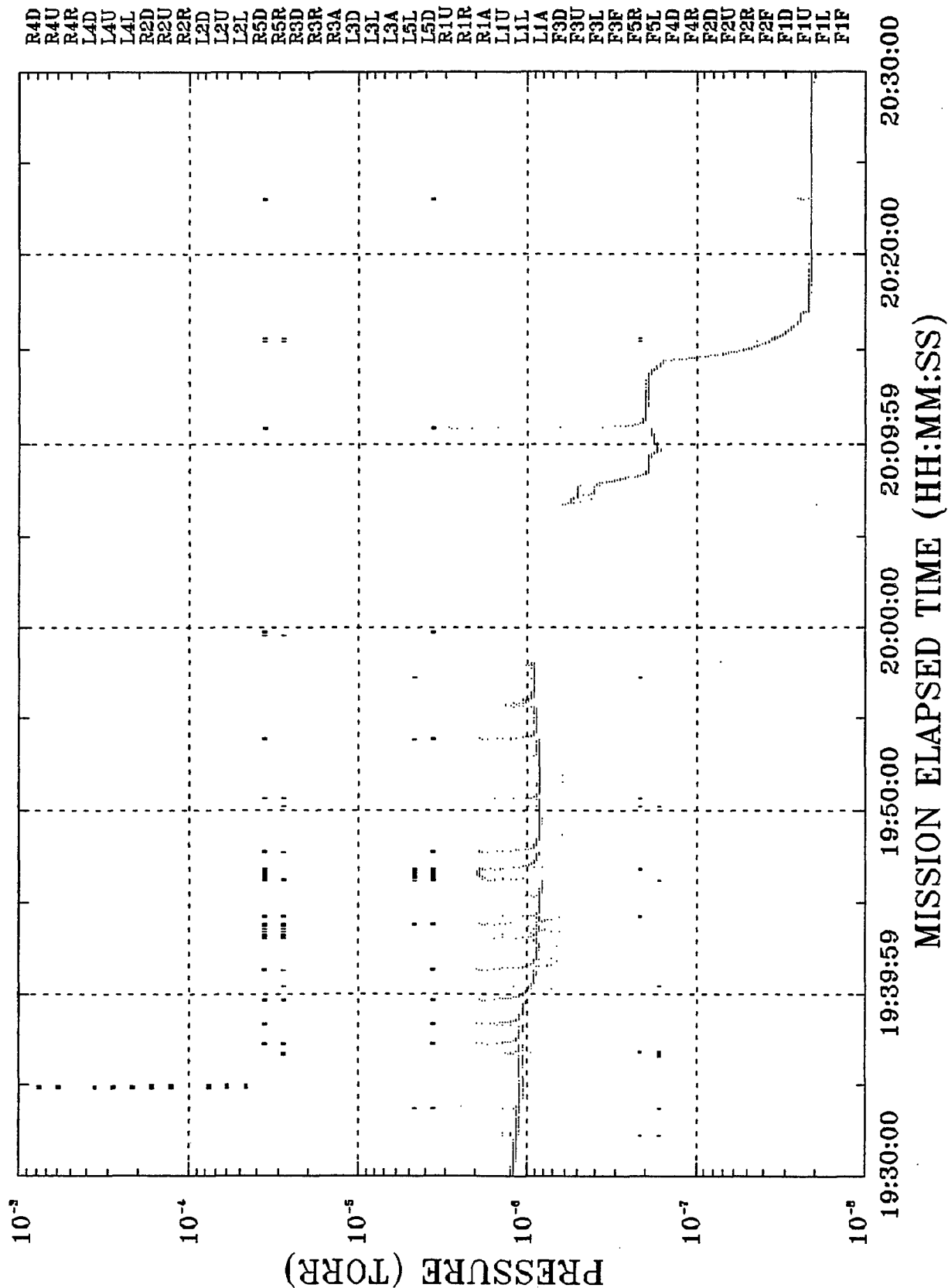


Figure 11. Pressure Measurements Made During the Initial Deployment of the SPAS on MET Day 2. Between 1930 and 2030 MET the SPAS was sequentially grappled by the RMS, hoisted out of the Shuttle's cargo bay, rotated about the RMS wrist joint, and released. Changes in the measured background pressures and amplitude of the thruster-induced pressures and amplitude of the thruster-induced pressure variations were observed during this time

30

MET. Also included in the plot is the thruster firing history in a format that was previously described. The SPAS was initially attached to the RMS between 1958-to-2006 MET, at which time the SPAS was electrically detached from the Orbiter power and telemetry systems. Immediately prior to these activities the measured pressure within the cargo bay was $10^{-6}$ Torr, consistent with this point in the mission. Thruster enhanced pressures were about a factor of 2 to 3 above the background which was also fairly typical of in-bay operations.

The SPAS was hoisted out of the cargo bay into a "low hover" position during the interval 2/2006-to-2009 MET. During this maneuver the relative orientation of the SPAS to the Shuttle coordinate system was unchanged. Thus the PG field-of-view was maintained towards the starboard as the instrument was raised above the sill of the bay. In the "low hover" position the PG was approximately 150 cm above the sill and "looked" out over the starboard wing. The measured pressures during this maneuver decreased by about a factor of 5 to approximately $2 \times 10^{-7}$ Torr. On the other hand, the thruster-enhanced pressure observed by the thruster firing sequence at 2011 MET was larger than comparable firings when the PG was within the cargo bay. The SPAS was held fixed in this "low hover" position until 2013 MET.

Starting at 2013 MET the SPAS was rotated about the wrist joint of the RMS. This movement changed both the position and the orientation of the PG relative to the Shuttle cargo bay. Since the grapple attachment for the RMS was located on the opposite end of the SPAS from the PG this rotation caused the instrument to move along a 5-m radius arc from the horizontal to an orientation where the PG pointed directly away of the cargo bay. The rotation was completed at about 2020 MET. In the PG's final orientation the background pressure within the antechamber was below the $2 \times 10^{-8}$ Torr sensitivity of the instrument. However, slight perturbations from RCS engines could still be detected even in this configuration (see 2023 MET).

The measurements obtained within this interval were consistent with the scattering of neutral gases within the cargo bay. As the PG was lifted out of the bay the obscuration of the instrument's field of view decreased but was non-negligible in the "low hover" position. The thruster-induced pressure enhancement at this location was larger, perhaps due to a more direct coupling to the scattered plume effluents. Only when the PG was rotated away from the bay did the measured background pressures decrease below the sensitivity of the instrument. However, even in this orientation the effects of the Shuttle's RCS were detected. We suspect that this response was due to scattering of the plume gases from structural elements on the SPAS that were within the PG's $2\pi$ field of view. Consideration of the scattering of thruster plume gases is considered in more detail in the next section.

31

## 4.8    Gas Pressure Variations Due to Controlled Gas Releases

During mission STS-39 there were several gas sources that produced short-lived pressure spikes within the Orbiter payload bay and near the SPAS during free-flyer operations. The most significant source of transient pressure spikes was the operation of the attitude control jets on the Orbiter and the SPAS. For in-bay operations, these pressure spikes were distinctly correlated with certain Primary and Secondary Reaction Control System (RCS) thrusters. The measured pressure spikes varied in amplitude depending upon the thruster in use and the geometry of the gas plume relative to Shuttle surfaces and the PG. Unfortunately a corresponding record of the SPAS' ACS was not available. However, the deployed measurements of pressure had large amplitude spikes that were associated with changes in the orbital attitude vector. Comparative pressure measurements were also made of the PG response to four separate CIV gases released from an associated Get-Away Special CANister (GASCAN) experiment operated several times during the mission. The PG data set was unsuccessfully reviewed for possible pressure variations due to waste water dumps, Orbital Maneuvering System (OMS) engines firings, and fuel cell purges. No pressure measurements were available during the CRO chemical releases at distant locations from the Shuttle. Finally, several clear examples of uncorrelated enhanced pressure transients were observed although the sources of the gas contamination were unknown. The effects of the attitude control jets and these other transient gas sources are discussed here.

### 4.8.1    TRANSIENT PRESSURE SPIKES RESULTING FROM RCS THRUSTER FIRINGS

The Shuttle Discovery has 44 RCS jets that are used for attitude control and translational maneuvers. These engines are located near the nose and tail sections of the Orbiter as illustrated in Figure 12. Table 2 is a list of the primary and vernier RCS engines including their thruster designations and other relevant data. The nominal thrusts for the primary and vernier jets are 870 lbs and 24 lbs, respectively. Typical burn times for the primary RCS engines vary from 80 ms to 150 s, operating in either a pulsed or steady-state mode as required. The vernier, or secondary, jets have fixed pulse widths of 80 ms with a maximum repetition frequency of 12.5 Hz (quasi-continuous). The RCS uses a fuel-oxidizer mixture of monomethyl hydrazine (MMH) and nitrogen tetroxide ($N_2O_4$). Typical combustion by-products are $H_2O$ (33%), $N_2$ (31%), $H_2$(17%) and CO (13%) with trace quantities of $CO_2$, $O_2$, and H [*Nicholson*, 1988; *Hunton*, 1994]. Unreacted or partially reacted fuel products are released while the jets are in operation. The RCS engines are

oriented to minimize the contaminant effects within the Shuttle payload bay from the exhaust gas plumes [*Nicholson*, 1988].

Figure 13 provides several examples of the measured pressure responses to sequences of RCS engine firings at various times throughout the STS-39 mission. The pressure data is plotted in 6 minute intervals along with the available RCS thruster history. The short vertical lines on each plot correspond to identified thruster firings within each second regardless of the emission mode; that is, pulsed or continuous. The associated engine designations are listed on the right hand side of the plot. Minor variations, on the order of a second, in the simultaneity of the PG response and the jet firings that can be seen in Figure 13 were due to the limited sampling rates of the PG and to the compressed RCS history files used for the survey plots. A more comprehensive listing of the RCS history for STS-39 was available and used in the detailed analysis of the PG pressure record. This higher resolution file had a temporal resolution of 80 ms.

The example in Figure 13a details the pressure response to a series of three identical engine firing sequences that occurred early in the mission near 1/0100 MET. The baseline pressures at the time of these observations was approximately $2\times10^{-6}$ Torr. In the repeated sequence the dominant pressure effect was due to simultaneous, 1-s continuous burns of the three, upward-pointing primary jets, the aft L1U and R1U and forward F1U engines. The combined effect of these jets caused the measured pressure within the payload bay to increase by a factor of 25 to about $5\times10^{-5}$ Torr. The 18-s sequences also had numerous secondary burns, including a nearly continuous burn of the L5D jets. The effects of the secondary engines were small compared to the pressure response to the primaries and to the magnitude of the baseline pressure. Unfortunately from this limited data it is difficult to ascertain whether the pressure responses were a superposition of independent gas plumes from each primary jet or due to the interaction of their respective plumes.

A second example is shown in Figure 13b for later in the mission on MET day 6. On this day as well as throughout the flight, the vast majority of attitude maneuvers were controlled by the secondary thrusters. The observed pressure perturbations resulting from these secondary jets were somewhat less than $2\times10^{-6}$ Torr. Thus early in the mission or at times when the payload bay was directed into the ram the effects of the secondary RCS jets were often obscured. A detailed consideration of the RCS jet history for the interval of Figure 13b indicated that most of the thruster firings were less than 1 s although there were several intervals of more extended firings. Although many of these firings included multiple jets, the largest pressure effects occurred when the R5D vernier thruster was operated. The pressure response to an extended RCS burn that

33
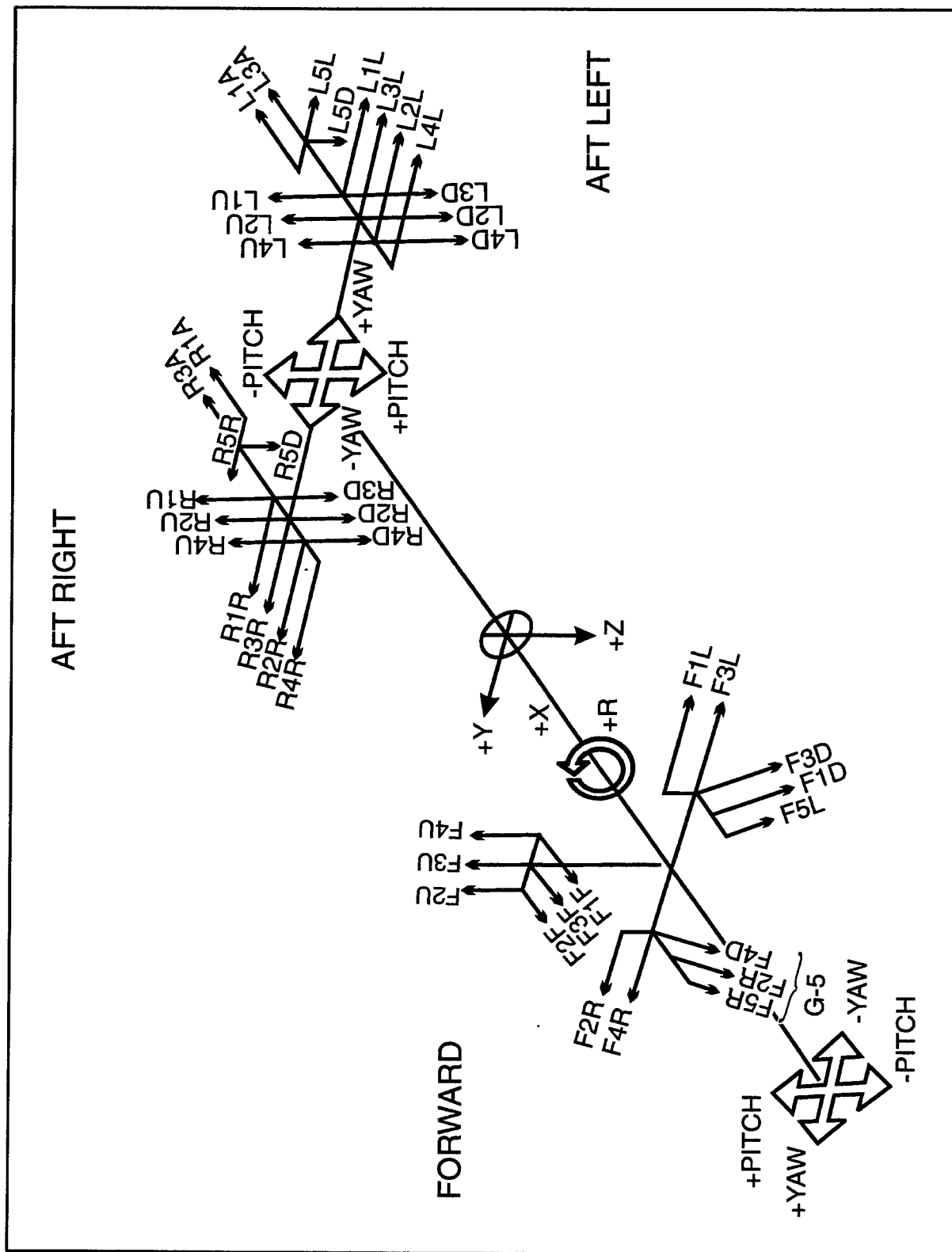
Figure 12. Schematic Illustration Showing the Locations of the RCS Engines and Thruster Directions. The Orbiter body axis coordinate system is noted in the sketch. The attributes of these engines are further discussed in Table 2

Table 2. Shuttle Reaction Control System Jet Designations.

| Jet[1] | Size | Jet[1] | Size | Jet[1] | Size |
|------|------|------|------|------|------|
| F1F | Primary | L1A | Primary | R1A | Primary |
| F1L | Primary | L1L | Primary | R1U | Primary |
| F1U | Primary | L1U | Primary | R1U | Primary |
| F1D | Primary | | | | |
| | | | | | |
| F2F | Primary | L2L | Primary | R2L | Primary |
| F2R | Primary | L2U | Primary | R2U | Primary |
| F2U | Primary | L2D | Primary | R2D | Primary |
| F2D | Primary | | | | |
| | | | | | |
| F3F | Primary | L3A | Primary | R3A | Primary |
| F3L | Primary | L3L | Primary | R3R | Primary |
| F3U | Primary | L3D | Primary | R3D | Primary |
| F3D | Primary | | | | |
| | | | | | |
| F4R | Primary | L4L | Primary | R4R | Primary |
| F4D | Primary | L4U | Primary | R4U | Primary |
| | | L4D | Primary | R4D | Primary |
| | | | | | |
| F5L | Secondary | L5D | Secondary | R5D | Secondary |
| F5R | Secondary | L5L | Secondary | R5R | Secondary |

[1]The three character designator for each engine is interpreted as follows:
1st - Engine location:          F = forward, L = aft left, R = aft right
2nd - Propellant manifold number
3rd - Thruster plume direction:     F = +$X$      R = +$Y$      D = +$Z$
       (Orbiter body axis)          A = -$X$      L = -$Y$      U = -$Z$


included the R5D jet occurred near 6/1049 MET.  During this 8-s burn the pressure initially increased to a steady-state level of $2\times10^{-6}$ Torr while the R5D vernier thruster fired alone for 2.8s. Simultaneously with the termination of the R5D thruster, the L5L, L5D, F5R, and F5L thrusters were fired.  In spite of the multiplicity of jet firings the pressure rapidly decreased after the end of the R5D thruster firing.  Thus, it is likely that the R5D exhaust plume scattered from the

Figure 13. Composite Plots of the Measured Pressure Responses and RCS Thruster History for 6-minute Intervals at Various Times Throughout the STS-39 Mission

Shuttle aft surfaces and eventually into the payload bay although the kinematics of the gas flow are unknown.

Aliasing of the pressure responses of the PG due to the mismatch between the small thruster pulse durations and the instrument sampling rate was a consideration in this analysis. It was previously mentioned that most of the pressure responses shown in Figure 13b were from RCS vernier thrusters firings of less than 1 s. The telemetry rate for the IBSS PG was 1.06 Hz with a sample-and-hold time for the analog-to-digital converters of less than 1 ms. Some of these short firings resulted in maximum pressure responses as large as the steady-state value indicated above. Specifically, the peak pressures measured at 6/1048.44, 6/1048.49 and 6/1048.72 MET which corresponded to respective thruster firings, including the R5D, of 0.62 s, 0.37 s, and 0.25 s were all on the order of $2 \times 10^{-6}$ Torr. This suggests that the time constant for achieving a "steady-state" pressure within the bay in response to a thruster firing was quite rapid, but with a decay time on the order of 1 second or longer.

The pressure responses to the thruster firing sequence indicated in Figure 13c contrast to the above. The detailed thruster history shows that the thruster firings responsible for the spiked pressure enhancements near 6/0017.5 MET were identical 0.5 s burns of the R5D and L5L jets yet the pressure responses differed and were clearly aliased. The steady-state pressure measured during an extended thruster operation, including the R5D jet, at 6/0014.5 MET, was $6 \times 10^{-6}$ Torr. During the 5-cycle thruster sequence after 6/0017 UT this maximum pressure was achieved only twice. This indicates that the time constants to steady-state and decay were apparently less than 1 s. The conclusion that we draw from the results from Figures 13b and 13c is that the time constant towards steady-state in the bay must have been close to 1 s.

Figure 13d is a record of the measured pressure within the cargo bay for an interval on MET day 0 for which no thruster history data were available. The observed pressure response was apparently due to a sequence of eight separate thruster firings of less than 1 s. We draw this conclusion based on the observation that the individual responses achieve slightly different peak pressures as in Figure 13c. Unfortunately the lack of a thruster history makes these conclusions speculative at best.

### 4.8.2 PRESSURE MEASUREMENTS DURING CIV GAS RELEASES

Several times during STS-39, controlled gas releases occurred within the cargo bay as part of the CIV investigation. The CIV experiment was a test of the theory of critical ionization that is attributed to *Alfven* [1954]. The basis of the theory is that a neutral gas traveling transverse to

a magnetic field, **B**, will undergo a non-classical ionization process if the transverse speed of the gas exceeds a certain threshold, $v^*$, given by,

$$v^* = 13.9 \text{x} \sqrt{E_i/m} \qquad [7]$$

where $E_i$ is the ionization potential of the neutral gas in eV, $m$ is the atomic or molecular mass in amu, and the 13.9 is a conversion factor. The critical ionization speed of the gas, $v^*$ is then in units of km s$^{-1}$ . Although Alfven's original hypothesis was that the CIV mechanism may have contributed to the formation of the solar system, more recently the role of CIV in the production of ions within the Space Shuttle environment has been considered [*Papadopoulos*, 1984; *Lai et al.*, 1988].

A set of five CIV experiments was conducted during STS-39. Each experiment consisted of the sequential release of four neutral gases and measuring the optical and plasma responses in the local environment. The gases released for the CIV tests, in order, were nitric oxide [NO: 7.7 km s$^{-1}$], Xenon [Xe: 4.2 km s$^{-1}$], neon [Ne: 14.4 km s$^{-1}$], and carbon dioxide [CO$_2$: 7.6 km s$^{-1}$] where the values inside the parentheses correspond to the speeds required for critical ionization for each of the respective gases. The nominal effluence rates for the gases were 0.1 mole s$^{-1}$ for NO and 0.25 mole s$^{-1}$ for the rest. These gases were released within the Orbiter's frame with the cargo bay facing towards ram. Various lighting conditions and orientations relative to the local magnetic field were used. The speed of the gas releases relative to the magnetic field was 7.7 km s$^{-1}$ plus the nozzle speed of the gas which was on the order of the gas thermal speed of several hundred m s$^{-1}$. Thus depending upon the orientation of the local magnetic field to the gas velocity, three of the four gases may have met the criteria for CIV.

The primary conclusion drawn from the CIV experiment on STS-39 was that the gas releases did not clearly induce the CIV mechanism [B.D. Green, private communication, 1993]. However there was an indication that some of the precursors to CIV may have been present [*Murphy et al.*, 1993]. Table 3 lists the times and configurations for the five CIV experiments and provides some brief comments on each. Note that PG data was available for only three of the experiments and that these releases occurred while the SPAS was either within the cargo bay or attached to the RMS. Although CIV may not have occurred the emitted gases did cause changes in the neutral-gas environment near the cargo bay. Pressure measurements obtained during CIV 3, 4, and 5 are plotted in Figure 14. For comparison purposes we have also included in this plot the CIV instrument nozzle pressures during the second release [Babcock, private communication].

The pressure perturbations measured by the PG for each of the CIV gas release sequences shown in Figure 14 were well defined and unambiguous. However, there were significant variations in the measured responses to the separate gases within each sequence and among the

Table 3. Critical Ionization Velocity (CIV) Gas Releases.

| | Start[1] | Experiment | Comment |
|---|---|---|---|
| 1. | 3/23:27 | Night Parallel | SPAS deployed - no PG data available. |
| 2. | 3/23:44 | Day Perpendicular | SPAS deployed - no PG data available. |
| 3. | 5/21:40 | Night Parallel | RMS operations - PG oriented towards bay. |
| 4. | 5/21:56 | Terminator Perp. | RMS operations - PG oriented towards bay. |
| 5. | 6/02:27 | Sunlit Parallel | SPAS in bay - RAM-Z at 90°. |

[1]Times for CIV 3-to-5 were derived from PG data.

different sequences. Some of these differences may have been due to the sensitivity of the cold-cathode gauge to the released neutral gases, as discussed earlier, and to changes in the nominal effluence rates from one sequence to the next. For example, *Babcock,* private communication, [1992] has noted that the Ne gas was rapidly expended during the first three CIV sequences although post-flight de-integration showed that all four bottles had positive pressures; that is, unreleased gases [Malonson, private communication]. In addition, the present results show that Ne gas effects occurred through the final sequence. The PG time history for CIV 5 also indicates that the cold-cathode gauge became contaminated during the Xe gas release and that the sensitivity of the PG was reduced until the end of the sequence, about a minute later. In spite of these difficulties it is possible to consider the trends that may have been due to geometric and lighting (daytime or nighttime) considerations of the gas releases alone.

The CIV 3 and 4 were conducted with the PG suspended above and "looking" down into the ram-facing cargo bay whereas the SPAS was located within the bay for CIV 5. Note that the high baseline pressures in CIV 3 and 4 resulted from fluxes of atmospheric gases scattered within the bay and into the field-of-view of the PG. The pressure perturbations due to the CIV gas sequences were similar except for a factor of two decrease in the pressure response to the Xe release after CIV 3. The two sequences differed in that the CIV 3 corresponded to a nighttime release parallel to *B* whereas CIV 4 was released near the terminator and perpendicular to *B*. On the other hand, the baseline for CIV 5 was considerably less than 3 or 4 owing to the attitude of the Shuttle in which the cargo bay was almost 90° from ram (refer to Figure 8b). Relative to these points, note that the perturbation caused by the Xe release in CIV 5 was slightly greater than
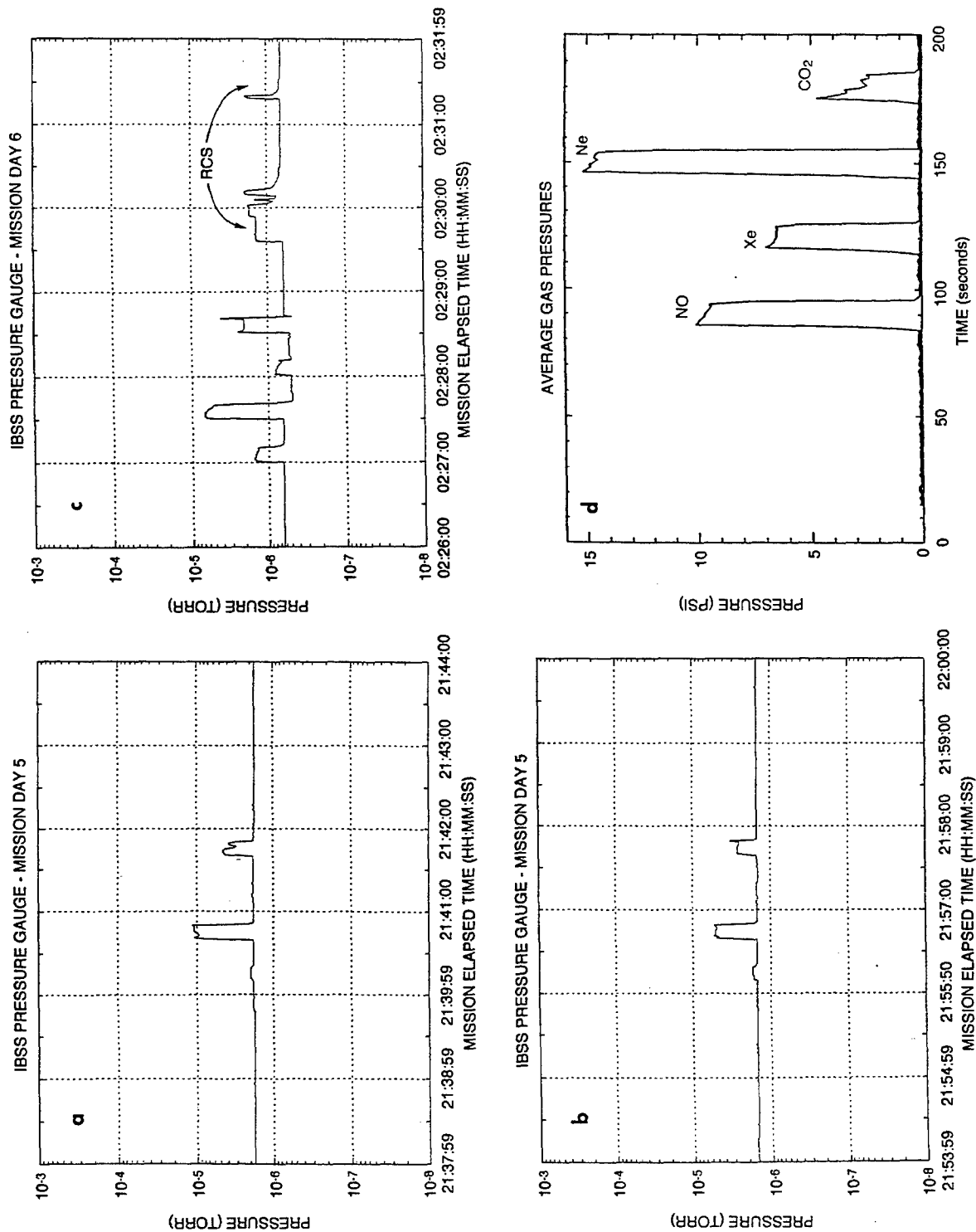
Figure 14. Pressure Measurements Made During Gas Releases for: a) CIV 3, b) CIV 4, and c) CIV 5. Panel $d$ is a plot of the pressure for CIV 2 measured within the CIV GAS canister, presented for reference purposes. [Babcock, private communication]

40

CIV 4 while the pressure response of NO and $CO_2$ remained the same. This implies that the effluence rates for Xe during the last three sequences were probably comparable. Thus, the differences in the pressure perturbations could be attributed to the distinct orientations of the gas flow to the magnetic field and, perhaps, the different lighting conditions. The implications of these results are beyond the scope of this report.

### 4.8.3 PRESSURE RESPONSES DURING OMS OPERATIONS, WATER DUMPS, AND FUEL CELL PURGES

The PG data were surveyed for pressure responses from potential contaminant gas sources on Shuttle. Tables 4, 5, and 6 respectively list the times of operations for the OMS, waste water dumps, and fuel cell purges during the STS-39 mission. Also included in some of these tables are brief comments related to the activities. These operations did not generate any identified perturbations in the measurements above the baseline pressures. We thus conclude that these sources were not a significant source of Shuttle contamination for STS-39. Similar results have been found for other Shuttle missions [*Shawhan and Murphy*, 1983].

### 4.8.4 GAS PRESSURE MEASUREMENTS DURING THE CRO EXPERIMENT

During the STS-39 mission three gas-filled canisters were deployed from the Shuttle and the gases subsequently released as part of the CRO experiment. The released gases were monomethylhydrazine (MMH) for CRO-A , unsymmetrical dimethylhydrazine (UDMH) for CRO-B, and nitrogen tetroxide ($N_2O_4$) for CRO-C. The gases were released only after the canisters had separated from the Orbiter by a considerable distance; that is, several tens of kilometers. The line-of-sight orientation of the canisters from the Shuttle was in a direction perpendicular to the Shuttle's orbital track. Table 7 lists the times of the deployment and release of the CRO experiment. Since the CRO gas releases occurred during telemetry blackout periods no PG data were available for comparison. As the data recorded by the PG during the CRO experiment becomes unclassified it will be possible to investigate Shuttle pressure responses to these gas releases. However, given the considerable separation distance between the Orbiter and the CRO canisters and the perpendicular orientation of the Shuttle's velocity vector to that of the separation vector it is unlikely that any effects were detected.

Table 4. Orbital Maneuvering System (OMS)-Times of Operation[1].

| MET | Duration | MET | Duration | MET | Duration |
|---|---|---|---|---|---|
| 0/00:10:42 | 057.4 | 3/10:23:53 | 032.9 | 3/20:55:53 | 022.3 |
| 0/00:36:14 | 131.3 | 3/10:30:53 | 022.6 | 3/21:00:53 | 021.6 |
| 1/01:00:39 | 001.3 | 3/10:35:53 | 021.0 | 3/21:12:53 | 000.1 |
| 1/01:04:37 | 001.3 | 3/10:47:53 | 002.6 | 3/21:22:53 | 023.1 |
| 1/01:04:06 | 001.3 | 3/10:57:53 | 023.9 | 4/01:32:53 | 031.2 |
| 2/20:51:07 | 009.1 | 3/11:04:53 | 022.7 | 4/02:10:07 | 006.5 |
| 2/21:21:07 | 000.7 | 3/11:09:53 | 021.8 | 4/03:47:03 | 032.9 |
| 2/22:01:07 | 002.9 | 3/11:31:33 | 023.6 | 4/08:03:59 | 009.9 |
| 2/22:21:07 | 008.2 | 3/14:29:07 | 002.9 | 4/08:59:53 | 011.8 |
| 2/23:45:53 | 003.3 | 3/17:58:53 | 007.6 | 4/09:47:26 | 008.3 |
| 3/00:45:53 | 001.8 | 3/18:54:53 | 012.6 | 4/10:07:26 | 003.3 |
| 3/05:00:07 | 010.5 | 3/19:19:53 | 004.0 | 4/23:05:42 | 013.2 |
| 3/07:20:07 | 012.3 | 3/19:44:53 | 005.5 | 4/23:54:27 | 012.9 |
| 3/08:49:53 | 010.4 | 3/19:59:53 | 009.5 | 5/11:40:07 | 009.7 |
| 3/09:31:52 | 030.7 | 3/20:14:53 | 020.4 | 5/12:24:59 | 009.6 |
| 3/09:49:53 | 012.0 | 3/20:21:53 | 022.4 | 7/04:20:07 | 014.0 |
| 3/09:56:53 | 022.5 | 3/20:26:53 | 021.3 | 7/10:53:36 | 004.6 |
| 3/10:01:53 | 021.3 | 3/20:38:53 | 000.1 | 7/21:21:28 | 011.2 |
| 3/10:13:53 | 002.5 | 3/20:48:53 | 023.3 | 8/06:20:27 | 145.5 |

[1]Reference: IBSS - 90-Day Assessment Report, dated August 30, 1991.

Table 5.  Waste Water Dumps[1].

|    | Start   | Stop    | Comment                                          |
|----|---------|---------|--------------------------------------------------|
| 1. | 1/17:52 | 1/18:37 | Data not continuous, no evidence of $H_2O$ dump. |
| 2. | 2/15:54 | 2/16:19 | Pressure data not available.                     |
| 3. | 4/17:27 | 4/18:20 | No evidence of $H_2O$ dump.                      |
| 4. | 6/21:09 | 6/22:04 | Data not continuous, no evidence of $H_2O$ dump. |
| 5. | 7/22:16 | 7/22:46 | Pressure data not available.                     |

[1]Reference: IBSS - 90-Day Assessment Report, dated August 30, 1991.


Table 6.  Fuel Cell Purges[1].

|     | Start   | Stop    | Comment     |
|-----|---------|---------|-------------|
| 1.  | 0/01:33 | 0/02:15 | No evidence |
| 2.  | 0/09:10 | 0/09:52 | No evidence |
| 3.  | 0/17:01 | 0/17:43 | No evidence |
| 4.  | 1/08:04 | 1/08:46 | No evidence |
| 5.  | 1/17:55 | 1/18:39 | No evidence |
| 6.  | 2/09:17 | 2/10:01 | No evidence |
| 7.  | 2/16:00 | 2/16:44 | No evidence |
| 8.  | 3/07:38 | 3/08:22 | No evidence |
| 9.  | 3/16:29 | 3/17:11 | No evidence |
| 10. | 4/07:31 | 4/08:12 | No evidence |
| 11. | 4/20:40 | 4/21:22 | No evidence |
| 12. | 5/11:51 | 5/12:33 | No evidence |

[1]Reference: IBSS - 90-Day Assessment Report, dated August 30, 1991.

Table 7.  Chemical Release Observations (CRO)[1].

|    | Deploy | Release | Comment |
|----|--------|---------|---------|
| 1. | 3/13:55 | 4/02:39:46 | CRO-C, Nitrogen tetroxide ($N_2O_4$) |
| 2. | 4/06:40 | 4/10:28:53 | CRO-B, Unsymmetrical dimethylhydrazine (UDMH) |
| 3. | 4/21:55 | 5/10:22:53 | CRO-A, Monomethylhydrazine (MMH) |

[1]Reference: IBSS - 90-Day Assessment Report, dated August 30, 1991.

## 5.    CONCLUSIONS

Neutral gas measurements obtained during  Space Shuttle mission STS-39 indicated that the baseline pressures within the cargo bay were substantially greater than the calculated atmospheric pressure of $4\times10^{-7}$ Torr.  These baseline pressures were determined by the attitude of the Shuttle relative to the ram and by outgassing products within the payload bay.  Elevated ram pressures of $2\times10^{-6}$ Torr resulted from the scattering of atmospheric gases within the payload bay.  There was a  remarkable similarity  in these measurements to the dynamic pressure  of  the direct atmospheric flow  which was measured  while the SPAS was deployed.  Payload bay pressures in the wake, on the other hand,  decreased continuously during the 7-day mission from a maximum of  $2\times10^{-6}$ Torr to $3\times10^{-7}$ Torr  with an outgassing decay time of  about 2.5 days.  The highest baseline pressures early in the mission peaked at several times $10^{-6}$ Torr due to a superposition of the outgassing products and the atmosphere.

Transient peaks in the measured gas pressure were due to Shuttle and SPAS attitude control thrusters and other controlled gas releases.  Within the payload bay the elevated pressures measured during RCS firings depended upon the thrusters in operation and on the baseline pressure level.   The magnitude of the pressure transients were dependent upon the availability of scattering surfaces within the exhaust plumes and the orientation of the PG  within the cargo bay.   On SPAS the PG had an unobscured field-of-view and apparently sampled the direct gas from the attitude control system.  These pressure responses at times exceeded the maximum capabilities of the PG of $2\times10^{-4}$ Torr.  Controlled gas releases during the CIV experiments were also observed during in-bay PG operations.  On the other hand, the PG did not detect any pressure variations from water dumps, fuel cell purges, or OMS operations.

# References

Ahmadjian, M., R.M. Nadile, J.O. Wise, and B. Bartschi, (1990) *J. Spacecraft Rockets*, *27*, 669-674

Ahmadjian, M., D.E. Jennings, M.J. Mumma, B.D. Green, B.D. Dix, and R.W. Russell, (1992) SKIRT Space Shuttle glow experiment, *J. Spacecraft Rockets*, *29*, 102-107

Allred, D.B., J.D. Benson, H.A. Cohen, W.J. Raitt, D.A. Burt, I. Katz, G.L. Jungeward, J. Antoniades, M. Alport, D. Boyd, W.C. Nunnally, W. Dillon, J.S. Pickett, and R.B. Torbert, (1988) The SPEAR-I Experiment: High voltage effects on spacecraft charging in the ionosphere, *IEEE Trans. Nucl. Sci.*, *35*, 1386-1393

Alfven, H. (1954) On the origin of the solar system, Oxford Univ. Press, New York, NY

Barengoltz, J. (1985) Gaseous background, in *Space Shuttle Environment*, edited by T.D. Wilkerson, M. Lauariente, and G.W. Sharp, pp. 223-226, Engineering Foundation, New York

Dubin, M., A.R. Hull, and K.S.W. Champion (Eds.) (1976) *U.S. Standard Atmosphere, 1976*, 227 pp., NOAA-S/T 76-1562, U.S. Government Printing Office, Washington D.C., 1976.

Erlers, H.K.F., S. Jacobs, L. Leger, and E. Miller (1984) Space Shuttle contamination measurements from flights STS-1 through STS-4, *J. Spacecraft Rockets*, *21*, 301-308

Erlers, H.K.F. (1984) An analysis of return flux from the Space Shuttle orbiter RCS engines, AIAA-84-0551, AIAA 22nd Aerospace Sciences Meeting, Jan. 9-12, 1984, Reno, NV

Goerke, R.T., P.J. Kellogg, S.J. Monson, R.C. Franz, R.J. Nemzek, H.R. Anderson, D.W. Potter, W.F. Denig, E.P. Szuszczewicz, and G.D. Earle (1992) Observations of VLF emissions from 50-mA electron beam injections in the ionosphere that are associated with beam-induced discharges, *J. Geophys. Res.*, *97*, 1319-1335

Green, B.D., G.E. Caledonia, and T.D. Wilkerson (1985) The Shuttle environment: gases, particles, and glow, *J. Spacecraft Rockets*, *22*, 500-501

Harris, J. (1991) Mechanical energy transfer in particle surface collisions, in *Dynamics of Gas-Surface Interactions*, edited by C.T. Rettner and M.N.R. Ashford, 1 pp., The Royal Society of Chemistry, Cambridge, U.K.

Hunton, D.E. (1994) Thruster firing effects in the Shuttle environment; 1. Neutral gas composition, *J. Geophys. Res.*, *99*, 3999-4009

Hunton, D.E. and J.S. Machuzak (1994) Thruster firing effects in the Shuttle environment: 2. Positive ion composition, *J. Geophys. Res.*, *99*, 4011-4022

Kawashima, N., M. Yanagisawa, S. Sasaki, K. Kuriki, T. Obayashi, T. Neuburt, P.R. Williamson, P.M. Banks, W.T. Roberts, D.L. Reasoner, W.W.L. Taylor, and J.L. Burch (1985) Vacuum and electromagnetic environment measured in SL-1 SEPAC, *ISAS RN 318*, 6 pp., The Institute of Space and Astronautical Science, Tokyo, Japan

Lai, S., W.F. Denig, E. Murad, and W.J. McNeil (1988) The role of plasma precesses in the Space Shuttle environment, *Planet. Space Sci.*, *36*, 841-849

Machuzak, J.S., W.J. Burke, J.M. Retterer, D.E. Hunton, J.R. Jasperse, and M. Smiddy (1993) Effects of thruster firings on the Shuttle's plasma and electric field environment, *J. Geophys. Res.*, *98*, 1513-1530

Miller, E.R. (984) Induced environmental contamination monitor - Preliminary results from the SpaceLab 1 flight, NASA TM-86461, 45 pp., Marshall Space Flight Center, Huntsville, AL, NTIS No N84-33461

Murphy, G.B., J. Wang, B.D. Green, and G. Caledonia (993) Evidence for critical velocity ionization in an ionospheric release experiment (Abstract), Paper SA42-D10, *EOS, Trans. AGU*, *74*, p 471

Narcisi, R., E. Trzcinski, G. Federico, L. Wlodyka, and D. Delorey (1983) The gaseous and plasma environment around Space Shuttle, *AIAA-83-2659*, Shuttle Environment and Operations Meeting, Oct. 31-Nov. 2, 1983, Washington D.C.

Nicholson, L.S. (1988) System description and design data - contamination environment - NSTS 07700, Volume XIV, Appendix 1, NASA

Papadopoulos, K (1984) On the Shutle glow (the plasma alternative), *Radio Science*, *19*, 571-577

Pickett, J.S., G.B. Murphy, and W.S. Kurth (1985) The gaseous environment of the Space Shuttle, *AIAA-85-6054-CP*, AIAA Shuttle Environment and Operations II Conference, Nov. 13-15, 1985, Houston, TX

Pickett, J.S., G.B. Murphy, and W.S. Kurth (1988) Gaseous environment of the Shuttle early in the Spacelab 2 mission, *J. Spacecraft*, *25*, 169-174

Redhead, P.A. (1959) The magnetron gauge: A cold-cathode vacuum gauge, *Can. J. Phys.*, *37*, 1260-1271

Riddleford, L. (1951) Notes on the ionization gauge, *J. Sci. Instrum.*, *28*, 375-379

Scialdone, J.J. (1983) Shuttle measured contaminant environment and modeling for payloads, *NASA TM-85111*, 13 pp., Goddard Space Flight Center, Greenbelt, MD, NTIS No. N84-12216

Shawhan, S.D. and G.B. Murphy (1983) Plasma Diagnostics Package assessment of STS-3 Orbiter environment and systems for science, *AIAA-83-0253*, AIAA 21st Aerospace Sciences Meeting, Jan. 10-13, 1983, Reno, NV

Shawhan, S.D., G.B. Murphy, and J.S. Pickett (1984) Plasma Diagnostics Package Assessment of the Orbiter plasma environment, *Journal of Spacecraft and Rockets*, *21*, 387-391

Selby, S.M. (1967) *Abridged Mathematical Tables*, 408 pp., The Chemical Rubber Co., Cleveland, OH

Trinks, H.and U. von Zahn (1975) The ESRO 4 gas analyzer, *Rev. Sci. Instrum.*, *46*, 213-217

von Zahn, U. and E. Wulf (1985) The gaseous environment of the Shuttle, as observed by mass spectrometer inside the payload bay of the Shuttle Orbiter, *AIAA-85-6097-CP*, AIAA Shuttle Environment and Operations II Conference, Nov. 13-15, 1995, Houston, TX

Wulf, E. and U. von Zahn (1986) The Shuttle environment: Effects of thruster firings on gas density and composition in the payload bay, *J. Geophys. Res.*, *91*, 3270-3278